JOURNAL OF GEOPHYSICAL RESEARCH, VOL. 86, NO. B4, PAGES 2825-2852, APRIL 10, 1981

Determination of Earthquake Source Parameters From Waveform Data for Studies of Global and Regional Seismicity

A. M. DZIEWONSKI, T.-A. CHOU, AND J. H. WOODHOUSE

Department of Geological Sciences, Harvard University, Cambridge, Massachusetts 02138

It is possible to use the waveform data not only to derive the source mechanism of an earthquake but also to establish the hypocentral coordinates of the 'best point source' (the centroid of the stress glut density) at a given frequency. Thus two classical problems of seismology are combined into a single procedure. Given an estimate of the origin time, epicentral coordinates and depth, an initial moment tensor is derived using one of the variations of the method described in detail by Gilbert and Dziewonski (1975). This set of parameters represents the starting values for an iterative procedure in which perturbations to the elements of the moment tensor are found simultaneously with changes in the hypocentral parameters. In general, the method is stable, and convergence rapid. Although the approach is a general one, we present it here in the context of the analysis of long-period body wave data recorded by the instruments of the SRO and ASRO digital network. It appears that the upper magnitude limit of earthquakes that can be processed using this particular approach is between 7.5 and 8.0; the lower limit is, at this time, approximately 5.5, but it could be extended by broadening the passband of the analysis to include energy with periods shorter that 45 s. As there are hundreds of earthquakes each year with magnitudes exceeding 5.5, the seismic source mechanism can now be studied in detail not only for major events but also, for example, for aftershock series. We have investigated the foreshock and several aftershocks of the Sumba earthquake of August 19, 1977; the results show temporal variation of the stress regime in the fault area of the main shock. An area some 150 km to the northwest of the epicenter of the main event became seismically active 49 days later. The sense of the strike-slip mechanism of these events is consistent with the relaxation of the compressive stress in the plate north of the Java trench. Another geophysically interesting result of our analysis is that for 5 out of 11 earthquakes of intermediate and great depth the intermediate principal value of the moment tensor is significant, while for the remaining 6 it is essentially zero, which means that their mechanisms are consistent with a simple double-couple representation. There is clear distinction between these two groups of earthquakes.

1. INTRODUCTION

In this paper we describe and illustrate applications of a procedure that could become an important tool in routine estimation of the principal seismic source parameters (hypocentral coordinates, seismic moment tensor) for earthquakes of moderate size. Considering the usual level of global seismicity, the analysis could eventually be applied to as many as several hundred events per year, rapidly transforming our level of understanding of the process of stress accumulation and release.

This scale of the analysis has become feasible because of the availability of the high-quality data from the recently established global digital seismic network. It is because of the potential impact of this development on the way in which earthquakes are studied that we wish to discuss briefly those aspects of the problem of quantification of earthquakes that pertain to estimation of the low-frequency characteristics of the source from the far-field data. A review of the subject of estimation of source parameters has recently been given by *Engdahl and Kanamori* [1980], who also discuss the problem of evaluation of the source time function, an issue that is not addressed directly in the applications described in this report.

The location of seismic sources is a routine task in seismology. The International Seismological Centre (ISC), for example, reports hypocentral coordinates for over 10,000 earthquakes each year. However, only a fraction of this number represents globally detected events. Because of the lateral variations in the earth's structure, the true uncertainty of the hypocentral parameters derived from the arrival times of the *P*-waves at teleseismic distances can be significantly greater than that indicated by the analysis of standard errors. Experiments with controlled sources show that errors of several tens of kilometers in epicentral coordinates are possible. Errors of similar magnitude can be expected for the estimates of the hypocentral depth.

Earthquake magnitudes, estimated from amplitudes of body waves (M_b) or short-period surface waves (M_s), are the most commonly determined parameters that characterize the size of an earthquake. Many seismologists find the concept of magnitude inadequate, partly because of the lack of a simple physical meaning, but the magnitude scale is so widely used that it is difficult to imagine that it would be readily abandoned. The standard magnitude estimates are meaningless for very large events [*Aki*, 1967; *Kanamori*, 1978] as the scale becomes saturated. In terms of the balance of the stress release, the concept of seismic moment [cf. *Aki*, 1966] is much more satisfactory.

Earthquake location and magnitude tell nothing about the nature of the forces that are associated with an event. This is the domain of 'source mechanism studies.' Usually, a great many assumptions, explicit and implicit, are associated with the usage of this concept. In the context of this study, which is focused upon the far-field, low-frequency effects associated with moderate size earthquakes, we shall essentially limit ourselves to the discussion of equivalent point sources.

Since the empirical evidence, combined with theoretical considerations, led seismologists to conclude that the 'double-couple' (plane shear stress) system of equivalent forces is the most appropriate model for most earthquakes, first-motion studies have usually been interpreted in terms of nodal plane solutions. Some basic discoveries were made by studying the signs of the first arrivals of body waves [cf. *Sykes*, 1967; *Isacks et al.*, 1968].

Paper number 80B1555.
0148-0227/81/080B-1555$01.00

Even though there must be, by now, several thousand published nodal plane solutions (*Denham* [1977] compiled data for 1713 earthquakes in the western and central Pacific alone), many of these results are of dubious quality. The basic difficulty is that the distribution of stations from which data are available is often inadequate to constrain both nodal planes. Also, routine determinations of the signs of the first arrivals, such as those reported in the ISC bulletins, are very frequently in error; for known nuclear explosions, the number of reported dilatational first motions is often comparable to that of compressional first motions. Thus reliable first-motion studies require the attention of a skilled researcher who personally examines the records, and consequently, the time spent is substantial.

An alternative approach to studies of the source mechanism is based on the analysis of radiation patterns of body waves, surface waves, and free oscillations of the earth. The theoretical background has been provided by, among others, *Ben-Menahem* [1961], who was the first to consider the finiteness of the fault and the effect of rupture propagation, and *Saito* [1967], who derived expressions for the excitation of surface waves and free oscillations of the earth for several types of equivalent systems of forces. The first estimation of the seismic moment from the excitation of long-period Love waves was made by *Aki* [1966] for the Niigata earthquake of 1964. *Kanamori* [1970*a*, *b*] proposed a procedure for the analysis of long-period surface waves generated by major earthquakes that has been subsequently applied to studies of the source mechanism and seismic moments of many of the important earthquakes of this century. *Langston and Helmberger* [1975] proposed a method of modeling the source using the waveform data of body wave phases and thus extended the analysis to much shorter periods.

The studies mentioned above involved, in the search for a best fitting double-couple model, a nonlinear inverse problem, in practice often solved by trial and error. An entirely new approach to the problem has been proposed by *Gilbert* [1971], who derived equations for the excitation of normal modes of the earth by the seismic moment tensor. Later, *Gilbert* [1973] suggested that since the amplitudes of normal modes excited by a seismic source are linear functionals of the six independent components of the seismic moment tensor, this property should be utilized in formulating the inverse problem for the source mechanism.

Dziewonski and Gilbert [1974] recognized the potential of this approach in removing the restrictive assumptions of the double-couple mechanism and analyzed a large number of manually digitized recordings of the Peru-Bolivia border earthquake of 1964 and the Colombian shock of 1970. The solution was obtained for a number of frequency intervals in an attempt to reconstruct the temporal history of the event. The details of their analysis and the theoretical background have been described, in a much broader context, by *Gilbert and Dziewonski* [1975] (hereinafter referred to as GD).

Buland and Gilbert [1976] and *Gilbert and Buland* [1976] proposed a variation of the approach described by GD: they compute the theoretical spectra for each of the six components of the moment tensor and then, in principle, can solve for the complex (in general) spectral value of the moment rate tensor at any frequency; in practice, this is accomplished by finding average values for finite frequency intervals.

There is a subtle but important difference between the method of *Dziewonski and Gilbert* [1974] and that of *Buland and Gilbert* [1976]. The former requires an extensive receiver coverage of the earth's surface (so that individual modes could, in effect, be isolated by the 'stacking' procedure and integration across a spectral peak could be performed) but is less sensitive to the departures of the structure of the real earth from that of the earth model used in the calculations of kernel functions. Also, it allows one to select the modes to be used in inversion, an important factor if one considers the fact that certain modes can be particularly strongly affected by lateral heterogeneities. The latter method is appropriate for a sparse receiver coverage but, at the same time, is more vulnerable to errors in the assumed earth structure and its departures from spherical symmetry. In this report we are using a sparse network, and the development presented here is essentially an extension of the method of Buland and Gilbert. However, we take steps to avoid some of the difficulties mentioned above.

There are by now many variations of the specific algorithm used to obtain a moment tensor solution from the waveforms of body waves, surface waves, or free oscillation data [*Stump and Johnson*, 1977; *Patton*, 1978, 1980; *Aki and Patton*, 1978; *Masters and Gilbert*, 1979; *Kanamori*, 1980; *Ward*, 1980; *Fitch et al.*, 1980]. The common element of all these methods is an a priori assumption of two sets of parameters: those of the earth's structure and those of the event location and the origin time. In practice, neither of the two sets of parameters is known precisely. We have attempted to perform the inversion in such a way as to minimize errors due to our imperfect knowledge of the earth's structure. If the same model is used in all inversions, these errors may tend to be systematic, resulting in a slight underestimate of the moment, for example; the location errors, however, are different for each earthquake, and they are likely to affect the individual solutions in a different way.

We describe in this report an approach that allows us to improve the location parameters and simultaneously to modify the solution for the moment tensor. This, in effect, yields the 'best point source' location, which for earthquakes of finite size need not be the same as the point of initiation of rupture. Ideally, one could, by comparison of this solution with that obtained from arrival times of short-period body waves, assess the spatial and temporal dimensions of seismic sources.

Our algorithm for the quantitative analysis of earthquakes was designed to satisfy the following requirements: (1) relative insensitivity of the results to the earth model used in the generation of the excitation kernel functions ('matching filters' in the terminology of *Buland and Gilbert* [1976]), (2) ability to investigate earthquakes of moderate magnitudes, rather than only exceptionally large events which are rare and unevenly distributed on the earth's surface, (3) 'objectivity' of the method, by which we mean that relatively few and preferably no subjective judgements need be made by an operator, and (4) reasonable numerical efficiency of the method, so that calculations can be carried out on a powerful minicomputer and data for a substantial number of events could be analyzed in a relatively short time.

In section 2 we show how we attempt to meet these requirements and illustrate application of the method to synthetic and real data. The results obtained from the analysis of 14 earthquakes can be used to draw initial inferences with respect to the potential of the method in application to the studies of global seismicity.

In section 3 we present the results of our analysis of the

foreshock and the series of aftershocks of the Sumba earthquake of August 19, 1977, (often referred to as the Indonesian earthquake)—an example of an interesting seismological and tectonic problem that could not be approached using the ultra-long-period data, as the events involved were too small. This illustrates the applicability of the method to investigations of regional seismicity.

In the concluding section (4) we summarize our findings and discuss potential future developments.

2. Inversion of Waveform Data for Seismic Source Mechanism

a. *General Considerations*

At present, there are in operation approximately 15 seismic research observatories (SRO) and abbreviated seismic research observatories (ASRO): Figure 1 shows their worldwide distribution. The sensors (for details, see *Peterson et al.* [1976]) are placed either in a borehole (SRO) or in a pressurized vessel in a seismic vault (ASRO). The long-period channels are sampled at a rate of 1 sample per second; the peak magnification of the ground motion is at 25-s period. Because of the sensitivity of these instruments (nominal dynamic range of SRO stations is 120 dB), they yield recordings with an adequate signal-to-noise ratio for long-period ($T > 45$ s) body waves for events as small as $M_b \sim 5.5$. This property is important, as in this work we intend to study the source mechanism using the body wave portions of seismograms.

For a typical epicentral distance of about 90°, the interval between the emergence of the *P*-wave and the arrival of the fundamental mode Rayleigh waves is approximately 40 min; for the transverse component this time is somewhat shorter, since fundamental mode Love waves travel with higher group velocities. Such an interval of a record contains in addition to the *P*- and *S*-wave arrivals also multiple reflections of these waves, converted phases, core reflections and, of course, all the phases including the primary *p* and *s* surface reflections. Thus the excitation of the seismic waves, contained in our hypothetical recording, projected back onto the focal sphere would yield information not about a single point on that sphere, as is usually the case in focal mechanism studies or waveform analyses limited to individual phases, but about the entire meridional section.

Little seems to be gained, unless excitation at very long periods is the subject of study, from extending the analysis to greater times. Dispersion and the amplitudes of fundamental mode surface waves in a period range from 40 to 100 s are very sensitive to lateral variations in the earth's structure; body waves that arrive along the major arc are not likely to contribute much to the resolution of the properties of the source, and the effect of differences between the real earth and the model is likely to be accentuated.

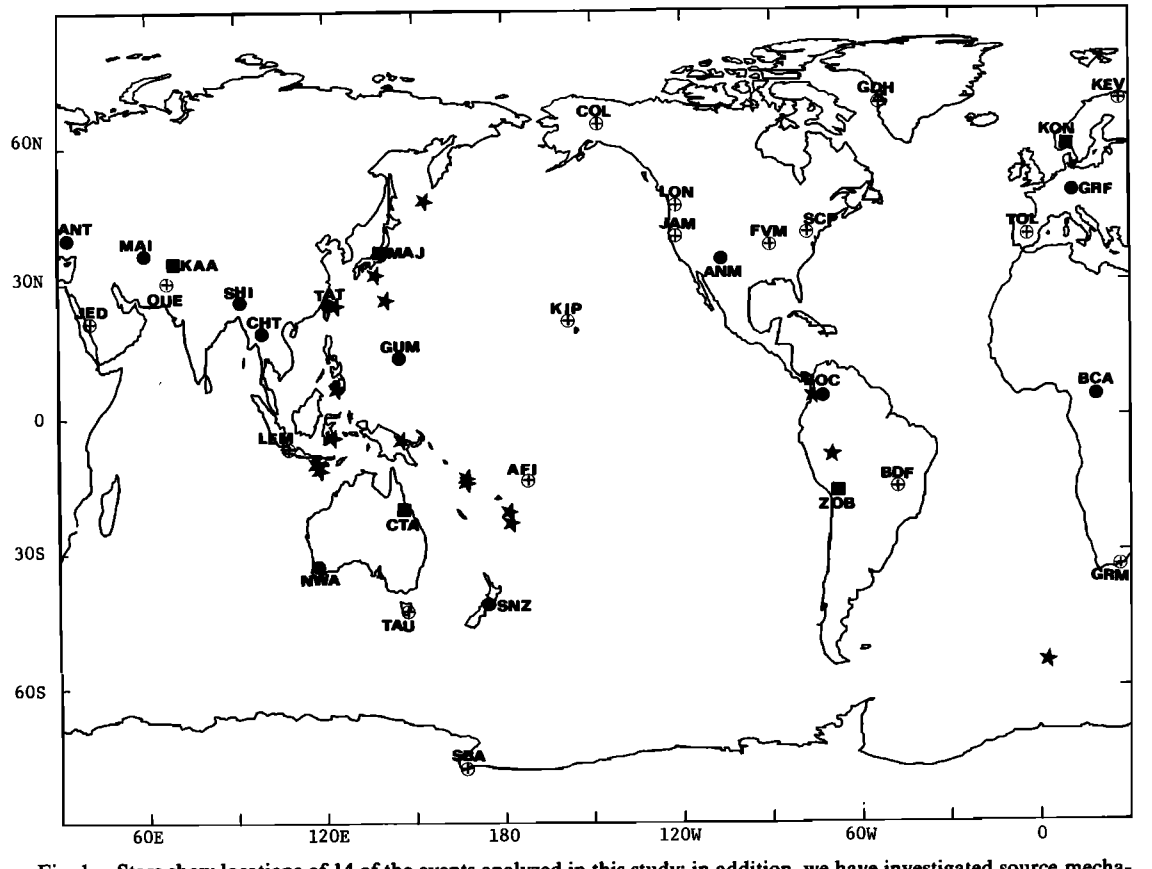

Fig. 1. Stars show locations of 14 of the events analyzed in this study; in addition, we have investigated source mechanisms of 11 events associated with the Sumba earthquake of August 19, 1977. Filled circles show the SRO and squares the ASRO stations operational at any time during the period from August 1977 to November 1979. Crossed circles are the proposed locations of the WWSSN stations which are to be equipped with digital data acquisition systems. Addition of those stations would greatly improve the azimuthal coverage; for all events analyzed here this coverage was rather poorly balanced.

Broadly, our strategy is as follows: having edited and filtered the data relating to a particular event, the time series are truncated at the times corresponding to the arrival of the first fundamental mode surface waves. The partial derivatives of the synthetic spectra with respect to the moment tensor components and hypocentral coordinates (the kernel functions) are calculated, and by an iterative least squares procedure convergence is achieved to the best fitting parameters.

The most straightforward method for construction of the kernel functions (synthetic seismograms and spectra) is that of superposition of normal modes. If all normal modes within the appropriate frequency range and group velocity window are used in construction of a synthetic seismogram, we are assured that no part of the theoretically predictable seismic signal has been omitted. Although the number of normal modes that are used in the summation is large, the computation times involved can be quite reasonable if a proper strategy is used.

The additional advantage of the normal mode method is its objectivity: the person processing records need not identify the phases in order to achieve correct results. This makes the approach suitable for essentially routine operations without the need for intervention by a skilled seismologist.

b. *Derivation of Excitation Kernels*

Following *Gilbert and Dziewonski* [1975], a component of ground motion excited by a point source may be expressed as

$$u_k(\mathbf{r}, t) = \sum_{i=1}^{6} \psi_{ik}(\mathbf{r}, \mathbf{r}_s, t) * f_i(t) \qquad (1)$$

where u_k is the kth record in the set of seismograms, with the receiver at position $\mathbf{r}$ and the source at $\mathbf{r}_s$. The excitation kernels ψ_{ik} depend also on the properties of the earth, both in terms of the displacement functions (eigenfunctions) of individual normal modes as well as their eigenvalues (complex frequency). Functions $f_i(t)$ represent the six independent components of the moment rate tensor, and we follow the notation used by GD: $f_1 = M_{rr}$, $f_2 = M_{\theta\theta}$, $f_3 = M_{\phi\phi}$, $f_4 = M_{r\theta}$, $f_5 = M_{r\phi}$, $f_6 = M_{\theta\phi}$; the asterisk signifies convolution.

Buland and Gilbert discussed the solution of (1) for $f_i(t)$ in the frequency domain representation, and there is no need to repeat their argument here. *Dziewonski* [1978*a*, *b*] pointed out that the excitation kernels can be efficiently calculated by first summing those contributions from all modes of the same angular order number, which are independent of the position of the receiver. Specific formulae, which essentially repeat the results of *Dziewonski* [1978*b*], are given in the appendix.

In Figure 2*a* we show a set of the excitation kernels, ψ_{ik}, computed for a deep source (580 km) and a three-component receiver at a distance of 98.8° and azimuth of 294.1°. The time functions shown in the figure were convolved with the response of an SRO instrument and low-pass filtered by a tapered filter with a cut-off period of 45 s. The catalog of normal

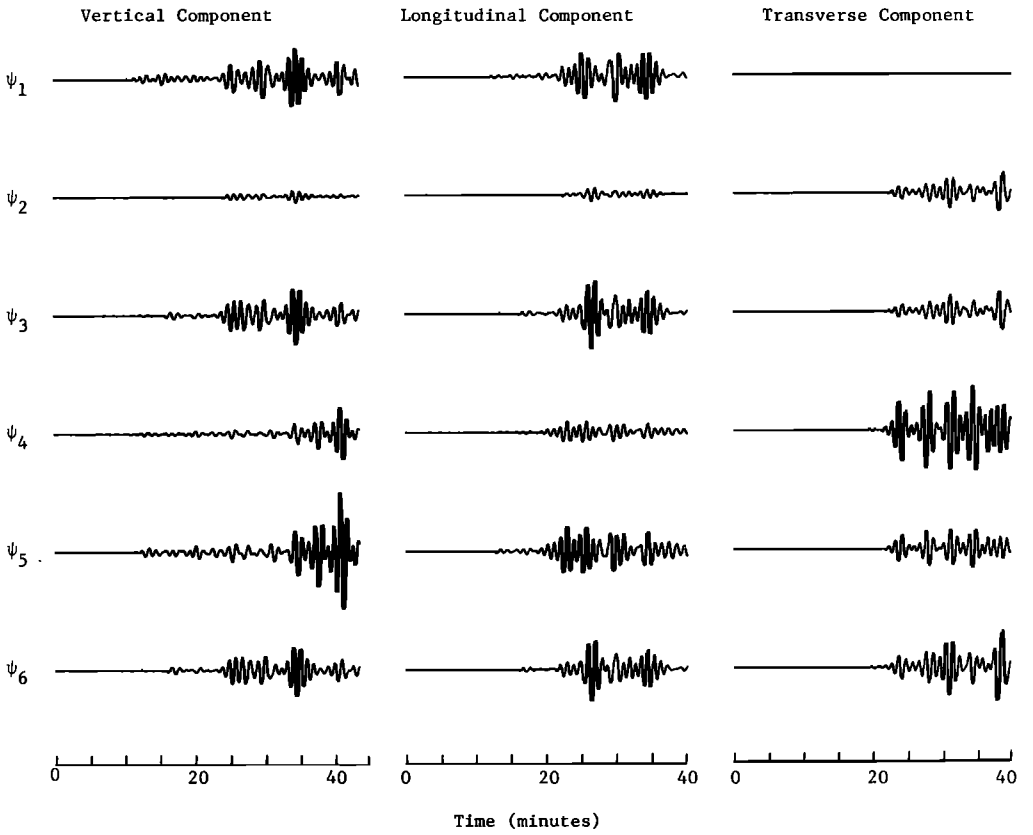

Fig. 2*a*. Excitation kernels for a deep earthquake (580 km) computed for the three components of the ground motion for a point on the earth's surface at a distance of 98.8° and azimuth 294.1° from the epicenter. The scale is common for all the traces in the figure. The traces represent synthetic seismograms excited by the individual components of the moment tensor of unit amplitude. A synthetic seismogram for an arbitrary point source is a linear combination of the six traces for a given component of the ground motion. The objective of our inversion procedure is to find the weights that give the best match between the observed and synthetic seismograms. Notice that there is a great diversity of shapes among the kernel functions. Intuitively, this indicates that for deep earthquakes, good resolution of the source properties could be achieved with relatively few recordings.

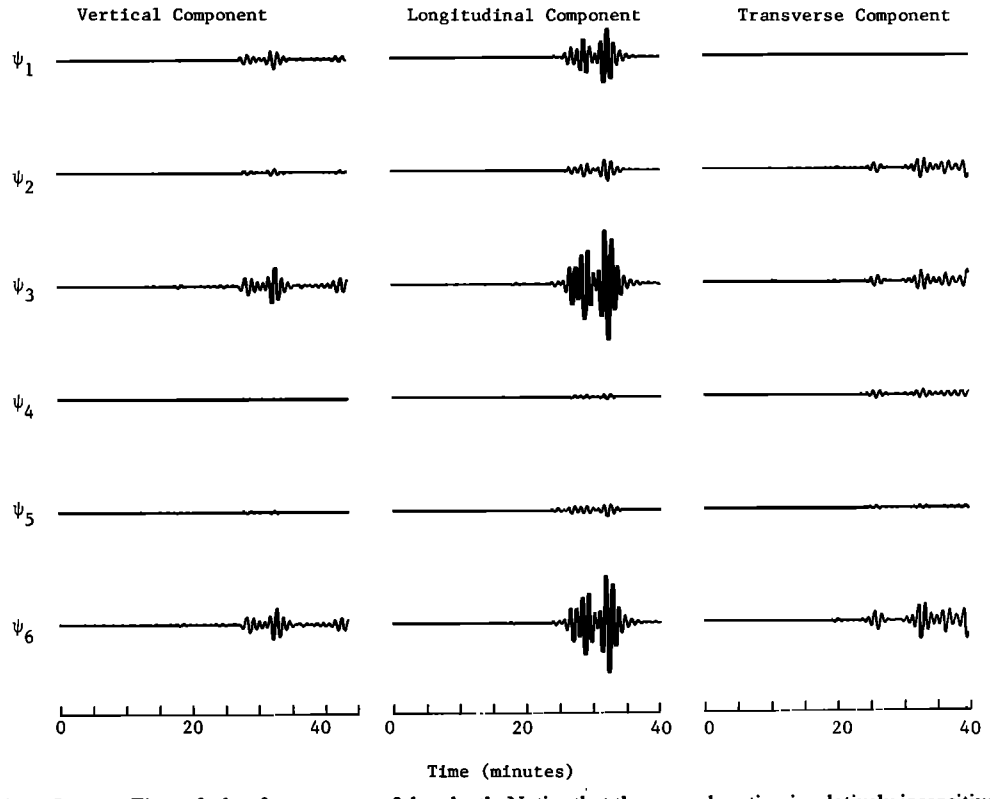

Fig. 2*b*. Same as Figure 2*a* but for a source at 3-km depth. Notice that the ground motion is relatively insensitive to the components f_4 and f_5 ($M_{r\theta}$ and $M_{r\phi}$). Also, for a given component of the ground motion the shapes of all synthetic traces are nearly identical. This means that (1) inversion with respect to the f_4 and f_5 (vertical dip-slip) elements of the moment tensor may be very unstable and (2) more extensive receiver coverage is necessary to obtain resolution for the remaining elements of the moment tensor. We would like to add, however, that the resolution for all elements of the moment tensor improves appreciably once the depth is greater than 10 km.

modes computed by *Buland* [1976] for an earth model 1066B (GD) was used in calculation of the traces in Figure 2*a* and throughout this paper. Attenuation coefficients were computed using model FSQMK of *Dziewonski* [1977]. It is quite clear that there is substantial diversity of shapes among the time functions representing the excitation kernels; it would not be unreasonable to expect that with a high signal-to-noise ratio and the reference earth model close to the real earth, a dependable point source mechanism could be derived from recordings at a single station [*Gilbert and Buland*, 1976].

The kernel functions for a very shallow source (3-km depth; Figure 2*b*) have significantly different properties. One characteristic feature is that the functions associated with f_4 and f_5 are very small (they become identically zero for a source at the surface); thus in the frequency range of our analysis it may be impossible to resolve the elements $M_{r\theta}$ and $M_{r\phi}$ for sources within the first 5–10 km ; below that depth the kernels are sufficiently large that adequate resolution can be expected. The other important characteristic of Figure 2*b* is that for a given component of the ground displacement all time functions appear to have an essentially identical shape; vanishing of the radial stress at the surface leads to a linear dependence between $\dot{U}$ and V/r, if $U/r \ll \dot{U}$. Thus resolution of the elements f_1, f_2, f_3, and f_6 would have to be achieved by additional geographical coverage.

Application of the procedure proposed by Buland and Gilbert to the system of equations of condition immediately following from (1) can lead to reliable solutions for the moment tensor if the estimated position of the source $\mathbf{r}_s$ and the origin time t_0 are correct, but this need not always be the case.

c. Perturbation With Respect to the Hypocentral Parameters: Iterative Solution

There are three reasons why the position of the source and the origin time estimated from the first arrivals of the *P*-waves may not be the best parameters to use in inversion for the moment tensor: (1) Representation of the source as a point in space and time is essentially correct, but the standard hypocentral parameters obtained from arrival times of *P*-waves are in error. (2) The hypocentral parameters are correct for the point of origin of rupture, but the source is distributed in time and space; consequently, the position of the centroid of the stress glut density [*Backus and Mulcahy*, 1976; *Backus*, 1977], the best point source, is incorrect. (3) Errors in the reference earth model or lateral heterogeneities, in conjunction with a particular distribution of stations, may lead to an apparent shift of the point source determined by radiation of long-period body waves. In reality, we deal with a combination of these three effects; all of them are of geophysical interest.

Assuming that we have an initial estimate of the moment tensor, $\mathbf{f}^{(0)}$ obtained by the procedure described in the previous section, we can expand (1) with respect to small perturbations in the source coordinates (r_s, θ_s, ϕ_s) and the origin time t_0. As the change in coordinates may lead to a different

moment rate tensor, we provide also for evaluation of these perturbations:

$$u_k - u_k^{(0)} = b_k \delta r_s + c_k \delta \theta_s + d_k \delta \phi_s + e_k \delta t_s + \sum_{i=1}^{6} \psi_{ki}^{(0)} * \delta f_i \quad (2)$$

where $u_k^{(0)}$ is the theoretical displacement calculated for the starting source coordinates and the initial estimate of the moment tensor, and b_k, c_k, and d_k, and e_k are the kernel functions:

$$\begin{aligned} b_k(t) &= \sum_{i=1}^{6} \frac{\partial \psi_{ki}^{(0)}}{\partial r_s} * f_i^{(0)} \\ c_k(t) &= \sum_{i=1}^{6} \frac{\partial \psi_{ki}^{(0)}}{\partial \theta_s} * f_i^{(0)} \\ d_k(t) &= \sum_{i=1}^{6} \frac{\partial \psi_{ki}^{(0)}}{\partial \phi_s} * f_i^{(0)} \\ e_k(t) &= -\sum_{i=1}^{6} \frac{\partial \psi_{ki}^{(0)}}{\partial t} * f_i^{(0)} \end{aligned} \quad (3)$$

The development outlined so far is general, and the excitation and location kernels could be obtained using any of the existing methods of construction of synthetic seismograms. The choice of the method will depend on the distance range and the part of the record that is selected for the analysis (*P*-waves or fundamental mode surface waves, for example).

In our approach the location kernels are obtained by summing the contributions from all relevant normal modes using the same strategy as described in section 2*b*. Specific formulae are given in the appendix.

The improved estimate of the moment rate tensor is again substituted into (2), after the kernel functions have been recalculated for the new location of the source, and the process is repeated until convergence is achieved.

We have performed the following numerical experiment in order to test the procedure. Synthetic seismograms were computed for a point source representing the superposition of an explosion with a strike slip earthquake ($f_1 = f_2 = f_3 = 1$; $f_4 = f_5 = 0$; $f_6 = 1$), placed at a depth of 580 km and geographical coordinates 21.50°S and 178.00°W. Also, the origin time has been delayed by 7.5 s with respect to an arbitrary t_0. The starting coordinates were $h = 600$ km, latitude 20.84°S, longitude 178.64°W, $t_0 = 0$ (these hypocentral coordinates correspond to those reported by the National Earthquake Information Service (NEIS) for an actual earthquake on April 24, 1979, which will be analyzed later in the report). Thus the starting location of the source is some 100 km away from the true position. The distribution of the stations used in this experiment is shown in Figure 3.

The results are listed in Table 1. The zeroth iteration yields a moment tensor that is very remote from the proper solution; even so, the first iteration brings about a major correction of the epicentral coordinates but the moment tensor shows very little improvement. With the new location some 45 km from the true coordinates, the moment tensor after the second iteration is within 93% of its expected value, and after four iterations the input parameters and the inversion results agree to five significant figures.

The conclusions from this experiment are the following: (1) Results of inversion for the moment tensor can be sensitive to the assumed location of the hypocenter. (2) Errors in estimates of the moment tensor are highly nonlinear functionals of the magnitude of mislocation of the source. (3) The process shows rapid convergence and stability, although there are obviously limits to how far the starting solution can be removed from the true one. Our example is close to that limit; from subsequent tests we have found that the solution does not converge if the mislocation vector is increased by 50%.

d. Application to the Analysis of Earthquake Data

1. *Preparation of the data.* Given an initial estimate of the location and origin time of an event, the data are read in for each of the stations beginning with a sample closest to the origin time and ending with a time corresponding to a group velocity of 3 km/s. Even though we do not use the fundamental mode surface wave data in our analysis, they are helpful in ascertaining the proper identity of the components. The demultiplexed traces are then filtered by a low-pass filter:

$$\begin{aligned} g(\omega) &= 1 \quad \text{for} \quad \omega \le \omega_1 \\ g(\omega) &= \cos^2 \frac{\pi(\omega - \omega_1)}{2(\omega_2 - \omega_1)} \quad \text{for} \quad \omega_1 < \omega < \omega_2 \\ g(\omega) &= 0 \quad \text{for} \quad \omega \ge \omega_2 \end{aligned}$$

The taper reduces the ringing effect associated with an abrupt truncation of the spectra; in our analysis we chose $\omega_1 = \pi/30$ and $\omega_2 = \pi/22.5$ s^{-1}. Of course, the equivalent procedure, in addition to the convolution with the instrumental response, is applied to the excitation and hypocentral location kernels.

After filtration, the traces are displayed on a graphics terminal, including the longitudinal and transverse components obtained by rotation of the N-S and E-W traces. As the Rayleigh and Love waves have distinct signatures, because of the differences in their group velocities, visual examination of the data helps to identify cases of erroneous multiplexing. We have encountered several such occurrences; they are listed in the third column of Table 2, for the benefit of other scientists who might use the data from the same station tapes. Also, obvious glitches, most frequently associated with the arrival of the *P*-wave, are eliminated at this stage by setting the starting and ending indices between which the sampled data from a particular trace are to be used in the analysis. Sometimes data for an entire trace are discarded.

The data selected in this preliminary editing process are then inverted for the moment tensor, with the principal objective of examination of the internal consistency of the data set. The preliminary estimate of the moment tensor is used to generate synthetic seismograms for comparison with the observations. This allows us to identify, for example, reversed polarities of components (the last column in Table 2) and glitches at times later than the first arrival. These are difficult to identify by visual inspection, as, in general, they could plausibly represent a part of the signal. It is our experience that the glitches are associated with the onsets of impulsive (as opposed to emergent) phases; the feedback mechanism is clearly unable to cope with abrupt changes in acceleration of the ground motion. It is not the magnitude but the sharpness of an arrival that seems to trigger this nonlinear behavior. Following this secondary editing, the data are inverted using the iterative procedure described in section 2*c*.

Because of the response of the SRO/ASRO instruments and our choice of the analysis of the early part of seismograms, the energy of the signal is strongly concentrated in a range of periods from 50 to 70 s. We have chosen not to consider the fre-

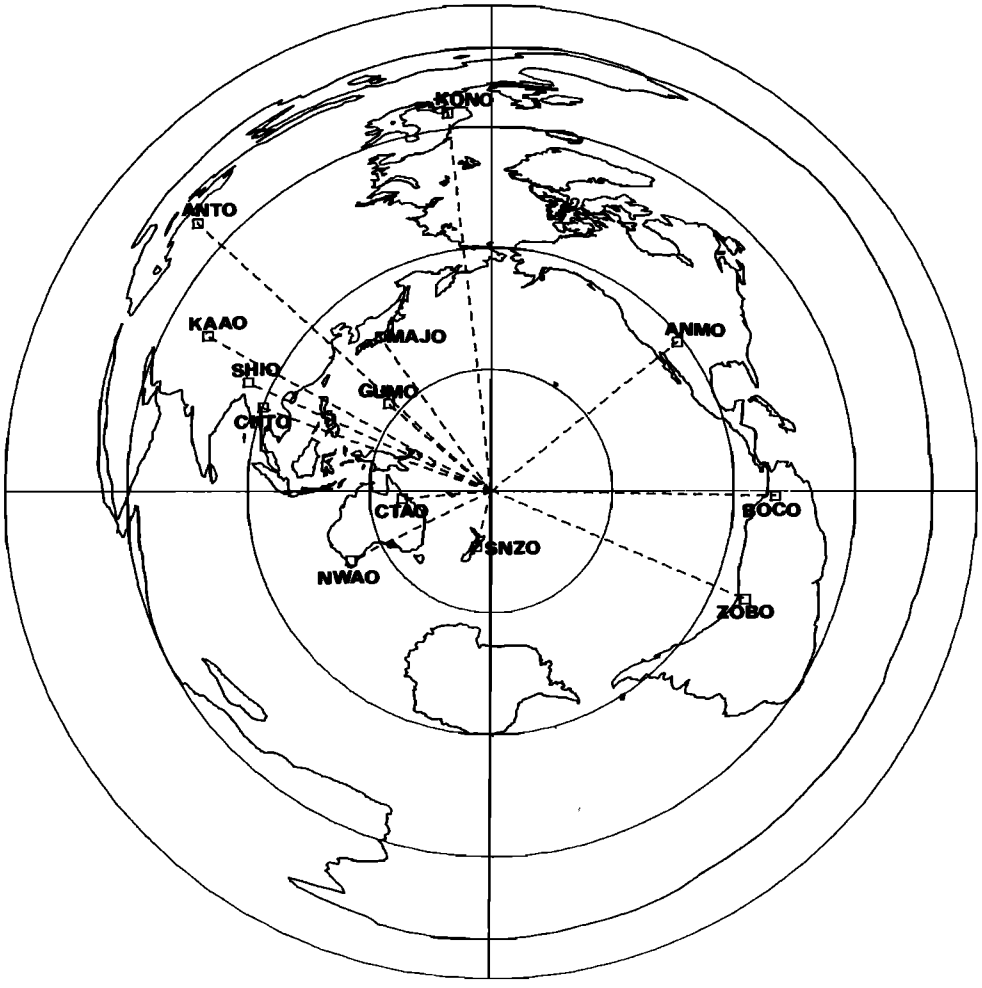

Fig. 3. Equidistant projection centered on the coordinates 20.84°S, 178.64°W showing distribution of the stations used in our experiment with the synthetic data. This location and station coverage corresponds to that for the event of April 24, 1979; the results of the analysis of the actual data for this earthquake are presented later in the text.

quency dependence of the moment rate tensor but to assume that the source time function is a step in time; because of the narrow band character of the signal, our solutions will be characteristic of the source spectrum at a period of approximately 1 min.

Another restriction has to do with our decision not to investigate the isotropic part of the moment tensor. Because the signal is dominated by the shear energy and all events analyzed in this study were clearly natural earthquakes, we felt that it was advantageous, at this exploratory stage, to impose the condition that the trace of the moment tensor must vanish: $f_1 + f_2 + f_3 = 0$.

2. *Event of September 23, 1978.* This is a fairly typical event among those analyzed in this study, and for this reason we selected it for a rather detailed description.

The parameters reported by the NEIS for this earthquake with M_b of 6.3 are the following: origin time 1632:11.1 GMT, epicentral coordinates 13.92°S, 167.21°E, depth 201 km; these data were used in the starting iteration. The distribution of stations is very similar to that shown in Figure 3, as the two events are only some 1500 km apart.

In Table 3 we list solutions obtained in successive iterations; as in the synthetic case, the most significant perturbations occur in the first and second iteration. The overall change in hypocentral coordinates is not very large: −0.02° in latitude, −0.31° in longitude, and −1 km in depth. However, the correction to the origin time is rather substantial: +9.4 s. We obtain positive δt_0 corrections for all analyzed earthquakes; the significance of this effect will be discussed in section 4.

The moment tensor is decomposed in terms of its principal axes; we list the eigenvalues as well as the directions of eigenvectors referred to the lower hemisphere of the focal sphere, as is customary in focal mechanism studies. For the purpose of comparison with the results of such studies we name the axis associated with the largest positive eigenvalue the 'tension axis,' the largest negative (in the sense of absolute value) the 'compression axis,' and the intermediate the 'null axis.' The latter need not be identically equal to zero, as we do not assume the source to be a double couple.

However, in the case shown in Table 3, after the final iteration the intermediate axis becomes zero, for all practical purposes, even though its value in the starting iteration was considerably larger. This decrease of the absolute value of the intermediate eigenvalue during the iterative process is very common, particularly for shallow earthquakes. Thus whatever is the cause for the discrepancy between the hypocentral location determined from the arrival times of short-period body waves and that obtained by inversion of long-period wave-

TABLE 1. Inversion for the Moment Tensor and Location of a Set of Synthetic Seismograms Computed for a Network of 12 Three-Component Stations (Figure 2)

	Interation				
	0	1	2	3	4
		Location			
Origin time, s	0.00	5.53	6.93	7.47	7.50
Latitude	20.84°S	21.10°S	21.40°S	21.51°S	21.50°S
Longitude	178.64°W	178.04°W	178.23°W	177.98°W	178.00°W
Depth, km	600.00	584.27	587.31	579.75	580.00
		Moment Tensor			
f_1	0.69844	0.71056	0.99344	1.00006	1.00000
f_2	0.33230	0.35757	0.97671	0.99992	1.00000
f_3	0.47704	0.51578	0.98099	1.00022	0.99998
f_4	−0.13696	−0.15316	−0.01460	0.00048	−0.00003
f_5	−0.02306	−0.09278	−0.00845	0.00034	−0.00001
f_6	0.14698	0.14584	0.93683	0.99946	1.00000
		Principal Axes			
Axis I					
Moment	0.76273	0.83205	1.91597	1.99995	2.00000
Plunge/azimuth	63/145	55/133	1/135	0/135	0/135
Axis II					
Moment	0.52791	0.49440	0.99317	1.00006	1.00000
Plunge/azimuth	24/293	32/287	89/300	90/	90/
Axis III					
Moment	0.21714	0.25246	0.04200	0.00061	−0.00001
Plunge/azimuth	13/28	12/25	0/45	0/45	0/45
Relative rms	0.84706	0.74561	0.16420	0.00175	0.00000

The parameters used in construction of the synthetic seismograms were origin time, 7.5 s; latitude, 21.5°S; longitude, 178°W; depth, 580 km; moment tensor, $f_1 = f_2 = f_3 = 1$, $f_4 = f_5 = 0$, $f_6 = 1$. The starting source location parameters are given in the column for iteration 0 (only the moment tensor is derived in the starting iteration); in the subsequent columns all entries correspond to the results obtained in a particular iteration.

form data, the iterative procedure seems to lead to conceptually simpler results (there are several earthquakes, however, for which we obtain a nonvanishing intermediate eigenvalue; in all cases when we think that the results are reliable, these are earthquakes of intermediate or great depth).

In Figures 4*a*–4*d* we compare some of the observed and synthetic seismograms computed using the source parameters obtained in the final iteration (Table 3). The amplitude scale is given in terms of the digital counts of an SRO instrument; the numbers in the figure correspond to the maximum amplitudes for a given pair of traces. Only the data bracketed by the vertical dashed lines were used in the least squares solution.

The quality of fit varies with time; at late times for distant stations it is often poor, while the resemblance of the observed and synthetic traces for the early part of the record, and entire records for close stations (for example NWAO and CTAO in Figure 4*b*), is very good. We have little doubt that the time dependence of the fit is caused by the lateral variations in the earth's structure. The energy observed at late times is primarily associated with multiply reflected body waves that spend much more time in the upper mantle and therefore are more sensitive to lateral heterogeneities. Records for stations MAIO, KAAO, and CHTO represent a good example. The azimuths at the epicenter are very similar for all three stations, but the paths to Meshed and Kabul cross the most tectonically active region of Asia. Although for early phases the agreement between observed and synthetic seismograms is good, the multiply reflected P-S_V waves show substantial differences at late times. For example, the synthetics for vertical and longitudinal components are 180° out of phase with respect to observed records at about 35 min after the origin time. On the other hand, the effect on S_H waves is much less, and the agreement is good throughout. The indication thus is that the differences are primarily related to P-S_V reflections and therefore may be of shallow origin. At the same time the agreement for Chieng-mai is good for all components.

In order to demonstrate that the results are not very sensitive to the misfits at late times, we have truncated the records when the disagreement between a synthetic and observed trace becomes severe. In Figures 4*a*–4*d* these times (always indicating the ending time) are shown by triangles. The important parameters of the solution are listed, together with those for 13 other earthquakes, in Table 4 as the second solution for the same date (event 7b). The differences are small: some 7 km in the location, 1 s in the origin time, a few percent in the eigenvalues, and extremely little change in the directions of the principal axes.

TABLE 2. Examples of the Erroneous Multiplexing or Reversed Polarities of Components Detected in Processing the Digital Data From the SRO/ASRO Network

Date	Station	Sequence of Components on Day Tape	Components With Wrong Polarity
Sept. 6, 1978	CTAO	Z, E-W, N-S	···
Sept. 6, 1978	TATO	N-S, E-W, Z	···
Sept. 15, 1978	SHIO	N-S, E-W, Z	N-S, E-W
June 25, 1979	BCAO	···	N-S, E-W
Aug. 5, 1979	NWAO	N-S, E-W, Z	···

TABLE 3. An Example of the Iterative Procedure Applied to the Analysis of the Waveform Data for an Intermediate Depth Earthquake in the New Hebrides Region on September 23, 1978

	Iteration				
	0	1	2	3	4
		Location			
Origin time	1632:11.1	1632:19.0	1632:20.0	1632:20.5	1632:20.5
Latitude	13.92°S	14.04°S	13.96°S	13.97°S	13.94°S
Longitude	167.21°E	167.12°E	166.92°E	166.91°E	166.90°E
Depth, km	201	198	201	200	200
		Moment Tensor			
f_1	1.090	1.152	1.295	1.345	1.341
f_2	−0.200	−0.192	−0.024	−0.159	−0.147
f_3	−0.891	−0.961	−1.271	−1.188	−1.194
f_4	−0.289	−0.172	−0.193	−0.200	−0.221
f_5	−0.346	−0.086	−0.142	−0.124	−0.134
f_6	0.774	0.544	0.503	0.508	0.504
		Principal Axes			
T axis					
Moment	1.285	1.186	1.342	1.388	1.390
Plunge/azimuth	66/141	80/153	79/153	80/153	79/154
N axis					
Moment	0.114	0.056	0.109	0.009	0.008
Plunge/azimuth	24/329	10/333	11/341	10/338	11/338
P axis					
Moment	−1.400	−1.242	−1.451	−1.397	−1.398
Plunge/azimuth	3/238	0/63	1/251	1/248	1/248
Relative rms	0.660	0.503	0.458	0.455	0.454

Starting source location parameters (NEIS monthly bulletin) are given in the column for iteration 0 (only the moment tensor is derived in the starting iteration); all entries in the subsequent columns correspond to the results obtained in a particular iteration. The results from the last iteration are entered into Table 4 as the final result for event 7a. The results for the moment tensor and its principal values should be multiplied by a scale factor of 10^{26} dyn cm.

It appears therefore that the solution is well determined by the early part of the recordings and that the discrepancies between the real, laterally heterogeneous earth and the model (1066B), which can become acute at late times, are unable to vitiate it; we shall discuss the implications of this conclusion in section 4. This finding is also confirmed by the results of experiments in which we have weighted the records by a factor t^{-1} (time elapsed after the origin time), thus giving much greater significance to early parts of recordings. For earthquakes with good S/N ratio, such weighting did not change the results appreciably. However, when the noise level is high, it may lead to serious distortions.

All the results presented in this paper were obtained using the least squares method with equal weighting. The standard errors have been computed using the usual formula, which applies to statistical models in which the errors are random and independent. This assumption is not entirely valid. The errors due to the discrepancies between the real earth and the model, and deviation between our point source model and a source distributed in time and space, may lead to systematic errors. In such cases the formal standard errors usually underestimate the real uncertainties. For example, the actual locations of known nuclear explosions are sometimes several standard deviations away from those obtained from the arrival times of *P*-waves reported by the global network. However, the relative uncertainties in determination of the individual components of the moment tensor depend on the geometry of station distribution and the depth of an earthquake, and for this reason the ratios of the standard errors are of interest.

Notice large glitches associated with the arrival of the *P*-wave at stations NWAO (Figure 4*b*), CHTO (Figure 4*c*), and TATO (Figure 4*d*); this is characteristic of SRO stations; ASRO stations do not show this effect. For example, the record from CTAO appears linear even though it is the closest station to the epicenter.

3. *Event of April 24, 1979.* This deep (600 km) earthquake provided some of the most spectacular examples of agreement between the observed and theoretical seismograms. In Figures 5*a*–5*c* we show examples from several stations characteristic of the azimuthal coverage; distribution of all stations is shown in Figure 2 (we have used the location of this event for the synthetic experiment described in section 2*c*). The azimuthal distribution of stations for this event is not well balanced: 8 out of 13 stations are in a single quadrant. This is the case for most of the earthquakes in the circum-Pacific belt. Addition of the proposed digital World-Wide Standardized Seismograph Network (WWSSN) stations (see Figure 1) would significantly improve the azimuthal coverage, and we consider early installation of these stations to be of significant benefit for scientific research.

Even though the moment of this earthquake was some 7 times smaller than that discussed in the previous section, the SRO records are not free of nonlinearities: there is a large glitch at station ANMO, at an epicentral distance of 88°. This station yielded a record of apparently good quality for an event 7 times larger and at comparable distance. This unpredictability of the nonlinear behavior of the SRO stations is rather puzzling.

The agreement between the observed and synthetic seismograms for this event is better than for any other case analyzed. We would like to draw the reader's attention to the vertical component records for stations SNZO and KONO; in the

TABLE 4. Results of Inversion for the Moment Tensor and Hypocentral Parameters for 14 Earthquakes

	Event 1, March 7, 1978	Event 2, March 15, 1978	Event 3, July 11, 1978	Event 4, Sept. 2, 1978	Event 5, Sept. 6, 1978	Event 6, Sept. 15, 1978	Event 7a, Sept. 23, 1978	Event 7b, Sept. 23, 1978
				NEIS				
Origin time	0248:47.6	2204:40.1	1217:7.8	0157:33.4	1107:43.1	1139:25.1	1632:11.1	1632:11.1
Latitude	32.01°N	26.42°N	7.89°S	24.90°N	13.32°S	48.25°N	13.92°S	13.92°S
Longitude	137.61°E	140.56°E	71.42°W	121.99°E	167.14°E	154.28°E	167.21°E	167.21°E
Depth, km	439	263	645	109	198	44	201	201
				Our Results				
δt_0, s	7.7 ± 0.3	3.5 ± 0.2	3.0 ± 0.4	7.6 ± 0.3	9.3 ± 0.2	2.6 ± 0.4	9.4 ± 0.3	8.2 ± 0.2
Latitude	31.52°N ± 0.02	26.34°N ± 0.01	7.91°S ± 0.05	24.50°N ± 0.02	13.31°S ± 0.02	47.73°N ± 0.03	13.94°S ± 0.02	13.88°S ± 0.01
Longitude	136.99°E ± 0.03	140.88°E ± 0.02	71.22°W ± 0.06	122.16°E ± 0.03	166.67°E ± 0.02	155.77°E ± 0.05	166.90°E ± 0.02	166.93°E ± 0.02
Depth, km	420 ± 2.0	258 ± 0.8	652 ± 0.4	101 ± 1.0	190 ± 0.8	31 ± 1.5	200 ± 0.7	201
Scale Factor, dyn cm	10^{26}	10^{25}	10^{24}	10^{25}	10^{26}	10^{25}	10^{26}	10^{26}
				Moment Tensor				
f_1	0.87 ± 0.08	−0.07 ± 0.07	−3.99 ± 0.30	1.35 ± 0.09	1.27 ± 0.03	1.15 ± 0.03	1.34 ± 0.03	1.46 ± 0.02
f_2	0.07 ± 0.10	−2.33 ± 0.12	0.74 ± 0.42	3.06 ± 0.15	−0.36 ± 0.05	−0.27 ± 0.03	−0.15 ± 0.04	−0.25 ± 0.04
f_3	0.94 ± 0.10	2.40 ± 0.13	3.25 ± 0.62	−4.41 ± 0.16	−0.91 ± 0.04	−0.88 ± 0.03	−1.19 ± 0.04	−1.21 ± 0.04
f_4	1.53 ± 0.09	−2.32 ± 0.10	−1.25 ± 0.21	1.71 ± 0.10	−0.28 ± 0.03	0.09 ± 0.05	−0.22 ± 0.03	−0.24 ± 0.03
f_5	−3.52 ± 0.11	−2.27 ± 0.09	4.42 ± 0.28	−1.59 ± 0.09	−0.79 ± 0.03	0.23 ± 0.06	−0.13 ± 0.03	−0.16 ± 0.03
f_6	0.47 ± 0.07	−3.77 ± 0.11	−1.83 ± 0.35	−1.50 ± 0.14	0.80 ± 0.05	−0.44 ± 0.03	0.50 ± 0.04	0.46 ± 0.04
				Principal Axes				
T axis								
Moment	3.9	4.7	6.2	4.7	1.6	1.1	1.4	1.5
Plunge/azimuth	52/66	13/65	24/246	32/16	64/127	84/286	79/154	80/152
N axis								
Moment	0.2	1.3	−0.1	0.2	0.0	0.0	0.0	−0.1
Plunge/azimuth	0/157	59/178	6/339	55/171	24/333	1/27	11/333	10/338
P axis								
Moment	−4.1	−6.0	−6.1	−4.9	−1.6	−1.1	−1.4	−1.4
Plunge/azimuth	37/247	28/329	65/83	12/278	11/239	6/117	0/248	1/248
Stations used	7	7	7	9	12	15	14	14

TABLE 4. (continued)

	Event 8 Oct. 1, 1978	Event 9, Dec. 18, 1978	Event 10, April 24, 1979	Event 11, May 13, 1979	Event 12, June 25, 1979	Event 13, Aug. 5, 1979	Event 14, Nov. 23, 1979
				NEIS			
Origin time	1323:50.1	1015:53.1	145:10.0	1730:56.8	529:5.6	053:54.8	2340:29.8
Latitude	6.68°N	54.48°S	20.84°S	4.05°S	4.98°S	22.72°S	4.80°N
Longitude	123.98°E	2.07°E	178.64°W	123.15°E	145.58°E	177.51°W	76.22°W
Depth, km	46	10	599	615	189	250	108
				Our Results			
δt_0, s	3.0 ± 0.3	8.2 ± 0.3	3.2 ± 0.2	2.9 ± 0.3	10.0 ± 0.2	2.9 ± 0.2	3.5
Latitude	6.71°N ± 0.04	54.69°S ± 0.03	20.79°S ± 0.02	4.05°S ± 0.02	4.93°S ± 0.02	22.93°S ± 0.03	4.86°N ± 0.02
Longitude	124.34°E ± 0.03	2.63°E ± 0.04	178.61°W ± 0.02	122.95°E ± 0.03	145.60°E ± 0.03	177.63°W ± 0.02	75.59°W ± 0.03
Depth, km	15 ± 1.3	10	600 ± 1.7	616 ± 1.8	191 ± 0.8	225 ± 1.0	116 ± 1.2
Scale Factor, dyn cm	10^{24}	10^{26}	10^{25}	10^{25}	10^{26}	10^{25}	10^{26}
				Moment Tensor			
f_1	4.56 ± 0.13	−0.08 ± 0.05	−1.83 ± 0.04	0.07 ± 0.02	−0.97 ± 0.03	−3.99 ± 0.12	−4.11 ± 0.13
f_2	−0.14 ± 0.16	1.40 ± 0.06	1.45 ± 0.07	−0.39 ± 0.02	0.50 ± 0.03	1.46 ± 0.24	−3.30 ± 0.24
f_3	−4.42 ± 0.18	−1.32 ± 0.06	0.38 ± 0.07	0.32 ± 0.02	0.47 ± 0.04	2.53 ± 0.20	7.41 ± 0.26
f_4	0.64 ± 0.38	−0.08 ± 0.05	−1.59 ± 0.06	0.26 ± 0.02	0.61 ± 0.02	−4.87 ± 0.13	−2.69 ± 0.12
f_5	−2.72 ± 0.76	0.30 ± 0.05	−0.61 ± 0.05	−0.98 ± 0.02	−0.22 ± 0.03	−4.27 ± 0.14	−3.92 ± 0.13
f_6	1.03 ± 0.14	0.07 ± 0.05	0.11 ± 0.05	0.10 ± 0.02	−0.48 ± 0.05	0.28 ± 0.16	1.18 ± 0.18
				Principal Axes			
T axis							
Moment	5.4	1.4	2.1	1.2	1.1	5.9	8.7
Plunge/azimuth	74/76	3/179	23/168	42/85	16/40	33/131	18/95
N axis							
Moment	0.0	0.0	0.4	−0.3	0.0	2.3	−1.6
Plunge/azimuth	0/67	77/281	5/76	17/339	11/307	5/224	31/196
P axis							
Moment	−5.4	−1.4	−2.5	−0.9	−1.1	−8.2	−7.1
Plunge/azimuth	15/257	13/88	66/334	43/233	71/185	57/321	53/339
Stations used	14	12	12	12	13	11	12

Entries 7a and 7b represent results of the analysis for the same earthquake but using different time windows. A finite duration of the source (24 s) has been assumed for event 14; accordingly, 12 s should be added to the value of δt_0 to obtain a result comparable to that for all other events in the table.

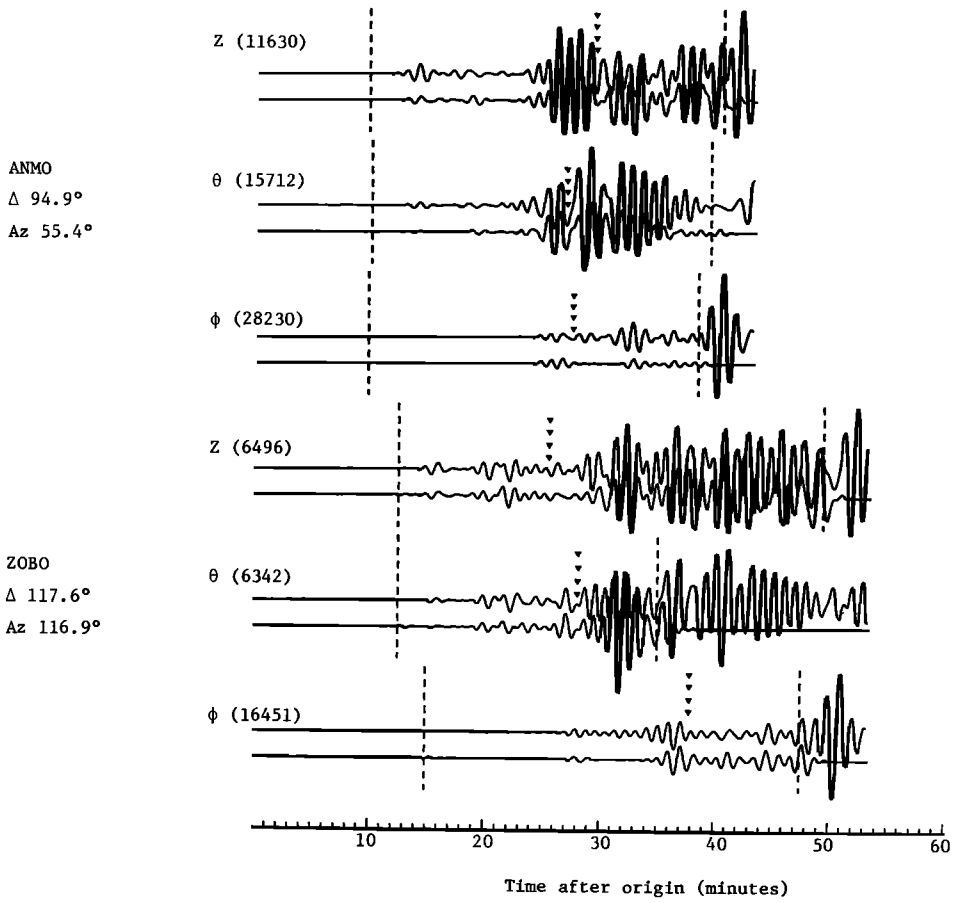

Fig. 4*a*. Comparison of the observed and synthetic seismograms for stations ANMO and ZOBO for an intermediate depth event of September 23, 1978. The top trace of each pair represents the observed seismogram; the bottom trace is the synthetic computed for the source mechanism listed in Table 4 as the entry for event 7a. The scale is common for each pair of traces. The numerical factor corresponds to the maximum amplitude for a given pair of traces. It represents the digital count of the SRO instruments; the ASRO response has been appropriately normalized. Only the data between the vertical dashed lines were used in the analysis. In order to investigate the possibility that the parts of records that show marked disagreement with the synthetics might vitiate our solution, we have truncated these segments of the time series; the new termination times are indicated by a set of triangles. This solution is entered in Table 4 as event 7b; the differences between solutions 7a and 7b are not significant.

former case the observed and synthetic traces are identical, for all practical purposes, but good reproduction of observed records for relatively small epicentral distances ($\Delta < 50°$) is fairly common. However, for station KONO ($\Delta = 141°$) the duration of the analyzed record is approximately 45 min, and yet the observed and synthetic records agree in all important details.

We think that the depth of an earthquake has much to do with this effect. Only rays corresponding to S to P converted phases can bottom above the source depth, and consequently, the synthetics are less sensitive to the details of the upper mantle structure. Relative steepness of the incidence angles at the surface also reduces the importance of P-S_V conversions which, we feel, are primarily responsible for the discrepancies between the observed and synthetic seismograms of the intermediate depth earthquake discussed in section 2*d*2.

There is, however, a systematic misfit that seems to be common to all records of longitudinal components observed at distant stations ($\Delta > 80°$), regardless of the source depth. The synthetics predict amplitudes systematically too low at late times. This cannot be explained by an error in the source mechanism or the Q-structure of the model, since we would not then expect satisfactory agreement for the vertical and transverse components. We think that the explanation must be related to some significant difference between the elastic properties of the upper mantle or the crust of the real earth and the model used in this study. This observation supports the view that the investigation of source mechanisms and the earth's structure cannot, and should not, be decoupled.

An interesting aspect of the result of the analysis for this event is the very small perturbation in the hypocentral parameters: only about 6 km in location and 3 s in the origin time.

4. *Event of March 7, 1978.* This deep event (439 km; M_b = 6.9; NEIS) was large enough to be well recorded by the instruments of the IDA network (international deployment of accelerometers [cf. *Agnew et al.*, 1976]). Thus it provides an opportunity to compare solutions obtained using an entirely different set of instruments, different range of periods, and different time span of analyzed records.

In Table 5 we compare our solution obtained from records of seven SRO/ASRO stations with that of *Masters and Gilbert* [1979]. Our moment is some 20% less than that obtained from

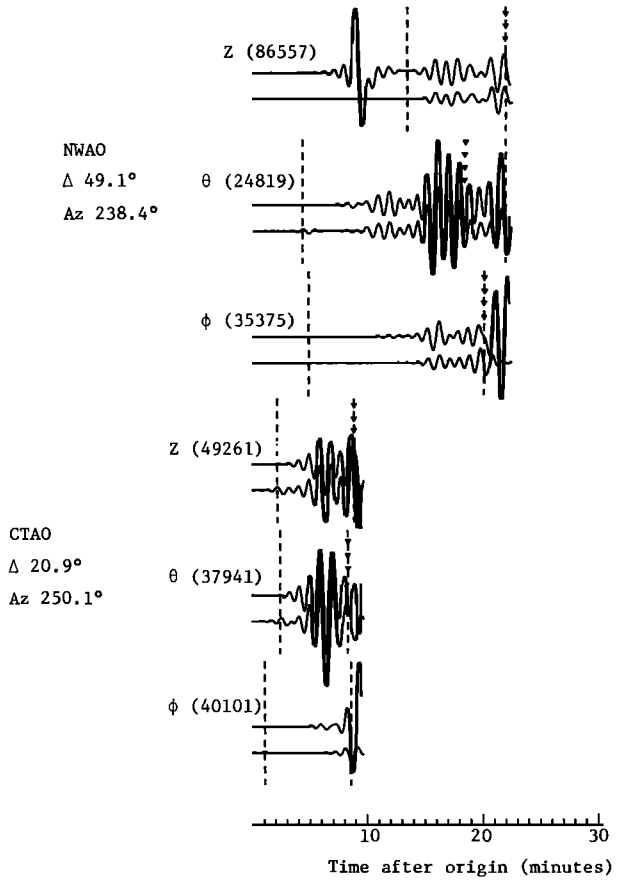

Fig. 4*b*. Same as Figure 4*a* but for stations NWAO and CTAO. Notice the glitch associated with the *P*-wave arrival on the vertical component of station NWAO. This is caused by the nonlinearity of the SRO instruments. CTAO, an ASRO station, does not show this effect even though it is much closer to the epicenter.

IDA data; this may be an effect of the finite duration of the source: 20 s would be sufficient to explain the difference. The plunges of the tension and compression axes are nearly identical, and their azimuths differ by 15°, on average; the solutions may thus be considered highly compatible. H. Kanamori (personal communication, 1980) informed us that his solution for this event, also based on IDA data but obtained using a different procedure, is similar to both solutions discussed above.

This means that combined capability of the global digital seismograph network for the high-quality analysis of seismic sources extends from events of seismic moment of the order of 10^{24} dyn cm upward.

Relatively large perturbations in hypocentral parameters should be considered with some caution, as the network coverage has not yet achieved its full strength; the average number of stations used to analyze earthquakes in 1979 was roughly twice that used in the analysis of the Honshu event.

5. *Notes on the analyzed events.* Table 4 summarizes results of our anlaysis for 14 earthquakes, arranged in a chronological order; three of these have already been discussed in some detail. Now we shall present a brief summary of the important characteristics of all the entries in the table.

Event 1: This event under the island of Honshu was discussed in section 2*d*4. Large perturbations in hypocentral coordinates are uncertain because of poor network coverage. Our moment tensor agrees with the results obtained using data from the IDA network.

Event 2: This was an intermediate depth event under the Bonin Island (M_b = 6.1; NEIS), with approximately 30-km shift in epicentral location; depth is decreased by 5 km. The source mechanism represents a superposition of a strike-slip (dominant) with a vertical dip slip; the M_{rr} component of the moment tensor is, essentially, zero. Intermediate eigenvalue is relatively large: 22% of the modulus of the largest eigenvalue.

There appears to be a tendency in the literature to decompose the set of principal values in terms of simpler mechanisms. This is a highly nonunique procedure which may tend to obscure the physical meaning of the solution. In the absence of the isotropic component the eigenvalues are $[\sigma_1, \sigma_2, -\sigma_1 - \sigma_2]$. From an infinite variety of possible combinations, two have achieved some popularity. Assuming that σ_1 and σ_2 are of the same sign and $|\sigma_1| > |\sigma_2|$, one decomposition is $[\sigma_1, 0, -\sigma_1] + [0, \sigma_2, -\sigma_2]$; often referred to as the 'major' and 'minor' double-couple systems. The other $[\sigma_1 + \frac{1}{2}\sigma_2, 0, -\sigma_1 - \frac{1}{2}\sigma_2] + [-\frac{1}{2}\sigma_2, \sigma_2, -\frac{1}{2}\sigma_2]$, represents a combination of a double couple with a 'linear vector-dipole' (LVD) [*Knopoff and Randall,* 1970; *Randall and Knopoff,* 1970]. Of course, one could write $[\frac{1}{2}(\sigma_1 - \sigma_2), -\frac{1}{2}(\sigma_1 - \sigma_2), 0] + [\frac{1}{2}(\sigma_1 + \sigma_2), \frac{1}{2}(\sigma_1 + \sigma_2), -\sigma_1 - \sigma_2]$, in which case the LVD component is maximized. Using the figures from Table 4 and a scale factor of 10^{25} dyn cm, these two alternative representations would be [5.35, 0, −5.35] + [−.65, 1.3, −.65] or [3, 3, −6] + [1.7, −1.7, 0], a major difference indeed.

We do not feel that such attempts at decomposition are particularly useful. One simple physical explanation of a nonvanishing intermediate eigenvalue is that the shear failure takes place on a curved surface and, subsequently, all three eigenvalues of the moment tensor assume finite values. Deviation from a simple double-couple mechanism can be effectively characterized by a parameter $\epsilon = |\lambda_{min}/\lambda_{max}|$; for a double couple, $\epsilon = 0$; for a linear vector-dipole, $\epsilon = 0.5$, the maximum for a moment tensor with no isotropic component. For this particular event, $\epsilon = 0.22$.

Event 3: This was the deepest of the analyzed events (652 km; M_b = 5.8; NEIS) but of rather small moment (6×10^{24} dyn cm) and relatively low signal-to-noise ratio. Our solution is similar to the nodal plane solutions obtained by *Isacks and Molnar* [1971] for earthquakes in the same region and comparable depths. Even though data for only seven stations were available for the analysis, the perturbation in epicentral coordinates is of the order of 20 km and 7 km in depth.

Event 4: This event was in north Taiwan (M_b = 6.1; NEIS), with an approximately 50-km shift in epicentral coordinates and an 8-km decrease in depth: a nearly perfect double-couple solution with a large strike-slip component.

Event 5: An intermediate depth event in the New Hebrides area (M_b = 6.0; NEIS), this is essentially a 'carbon copy' of the event discussed in section 2*d*2 (events 7a and 7b in Table 4). Both of these earthquakes have similar moments and orientation of the principal axes and, what is perhaps the most important, very similar perturbation in the epicentral coordinates. Thus even if our relocation procedure is biased by the lateral heterogeneities or erroneous features in the reference earth model, the relative locations appear to be highly reliable if the network coverage is good.

Event 6: This event in the Kurile Islands (M_b = 6.0; NEIS) had a major shift in epicentral coordinates; approximately 140

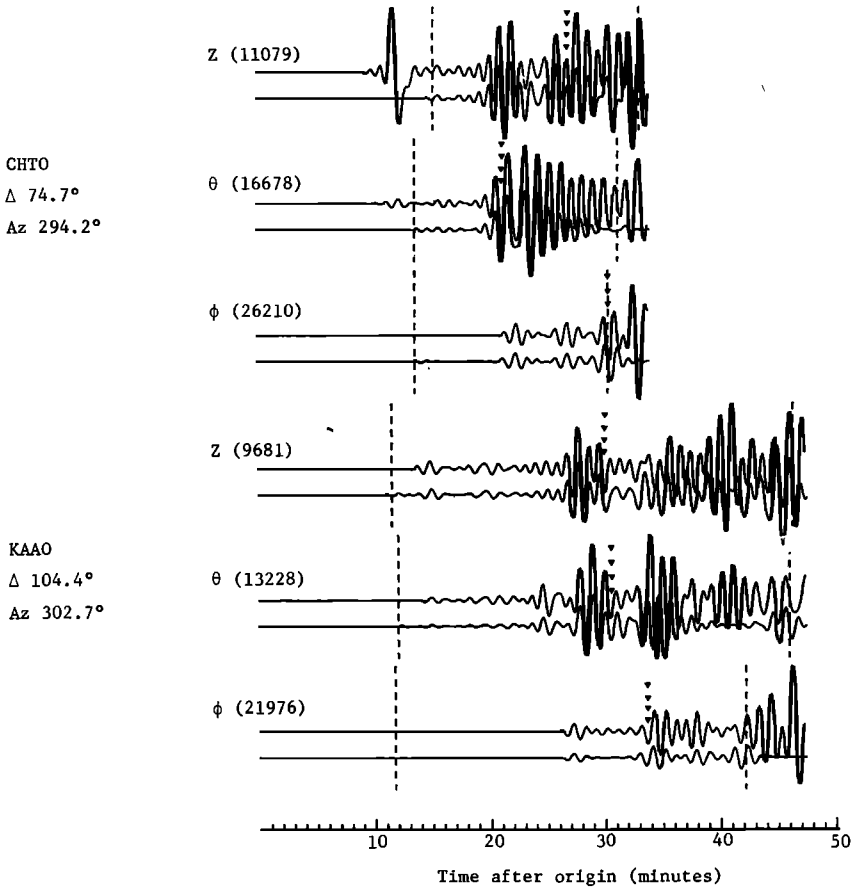

Fig. 4c. Same as Figure 4a but for stations CHTO and KAAO; nonlinearity is seen again at CHTO.

km to the southeast. It is a double-couple solution with the horizontal axis of compression perpendicular to the trench axis and nearly vertical axis of tension; the null axis is also horizontal and parallel to the trench axis. The final depth of this earthquake is 31 km (reduced from 44, reported by the NEIS). If our relocation of this event is correct, then it would be associated with the outer rise, and its mechanism (reverse faulting) would be consistent with the stress regime in the lower part of the buckled lithosphere [cf. *Chen and Forsyth,* 1978].

Event 7 (a and b): This event was already extensively discussed in section 2*d*2 and in conjunction with event 5. Event 7a corresponds to the analysis which included late segments of seismograms with, on occasion, an obvious disagreement between the observed seismograms and synthetics; these segments have been truncated in the inversion for which the results are presented as event 7b. The results are very similar, including the estimates of standard errors; the smaller average deviation obtained from the analysis of 7b has been offset by the reduced number of data points.

Event 8: This was a shallow event off the southwest coast of the Mindanao Island (M_b = 5.6; NEIS), with a major decrease in depth from the estimate given by the NEIS (reduction from 46 to 15 km). Notice that because of the shallowness of the event the errors associated with the f_4 and f_5 ($M_{r\theta}$ and $M_{r\phi}$) elements of the moment tensor are several times greater than those for other components. Even so, the normal fault mechanism is clearly dominant. The seismic moment (5×10^{24} dyn cm) is the smallest of all events analyzed in this study.

Event 9: This event near Bouvet Island in the South Atlantic can be characterized as a 'slow' earthquake, because of a large difference between the M_b (5.5) and M_s (6.5) magnitudes. This earthquake has been also analyzed by *Kanamori* [1980], who used the IDA data in his study of the excitation of long-period surface waves (200–300 s). His estimate of the seismic moment ($\sim 2 \times 10^{26}$ dyn cm) is higher than ours: 1.4×10^{26} dyn cm, which is consistent with the 'infrared' character of earthquakes associated with the spreading centers [*Kanamori and Stewart,* 1976]. There was a major change in epicentral coordinates reported by the NEIS in the Preliminary Determination of Epicenter (PDE) cards (55.4°S, 1.1°E) and in the monthly bulletin (54.47°S, 2.07°E). Our inversion procedure, in which we started with the PDE coordinates, converged to a location at 54.69°S and 2.63°E, some 40 km from the improved estimate but about 150 km from the initial PDE location. The mechanism is dominated by the strike-slip component. Despite a very shallow depth, fixed at 10 km, the f_4 and f_5 components remained stable.

Event 10: This deep event under Fiji Islands was discussed in section 2*d*3.

Event 11: This was a deep event under the Banda Sea (M_b = 5.7; NEIS). As for all deep earthquakes analyzed by us, the change in the hypocentral coordinates is rather small. This event had, we believe, a resolvable intermediate eigenvalue: ϵ = 0.22. The dominant component of the moment tensor is f_5, indicating that the slip occurred either in a nearly vertical or horizontal plane with the null axis pointing N20°W.

Event 12: This was an intermediate depth earthquake un-

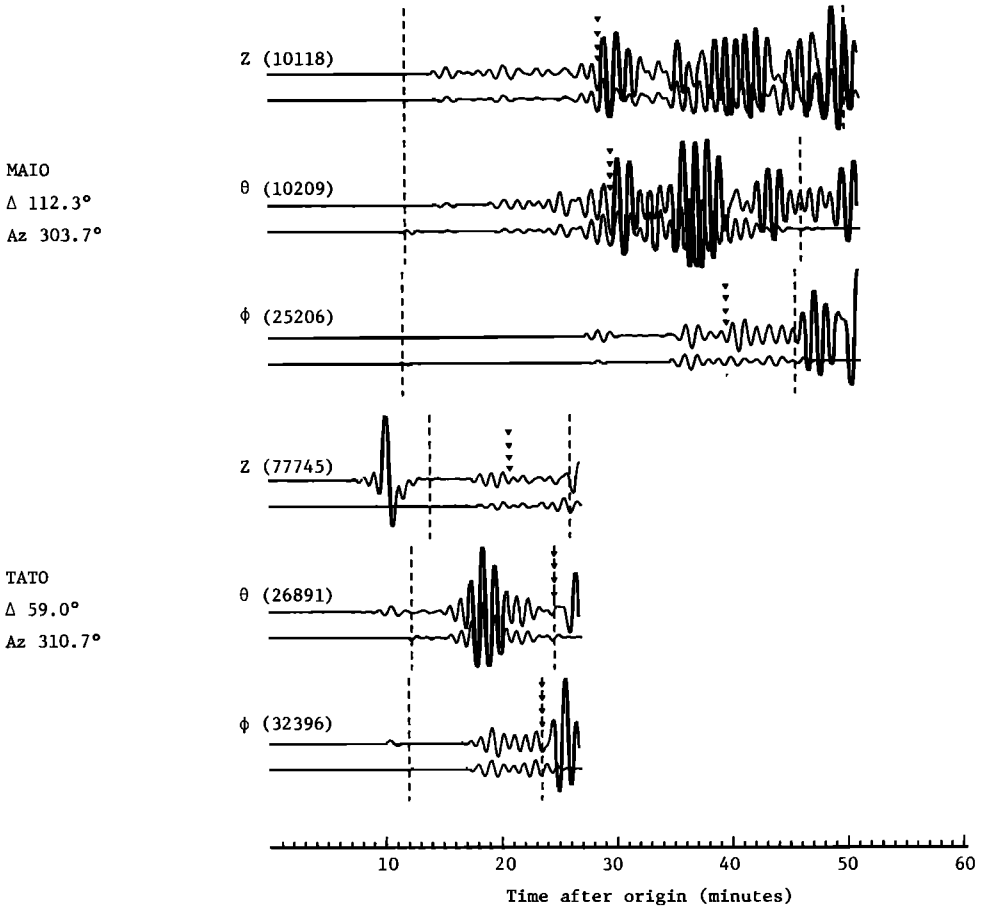

Fig. 4*d*. Same as Figure 4*a* but for stations MAIO and TATO. Notice the glitch on the vertical component of station TATO.

der New Guinea (M_b = 6.2; NEIS), with a simple double-couple mechanism.

Event 13: This was an intermediate depth event south of Fiji Islands (M_b = 6.4; NEIS). It is a rather complex earthquake with a particularly large intermediate eigenvalue: ϵ = 0.28, the largest of all events in this report. Excellent agreement between the observed and computed seismograms seems to indicate that this result is reliable. In Figure 6 we show records from two distant stations: ANTO (Δ = 149°) and GRFO (Δ = 152°); the observed and synthetic records agree in all important details. Notice that these two SRO stations exhibit nonlinear behavior even for *PKP* phases from this moderate size earthquake (moment ~7 × 10^{25} dyn cm).

Event 14: This earthquake (M_b = 6.4; NEIS) had the largest moment of all events analyzed in this report, and we obtain a significantly better fit to the data if we allow for a finite duration of the event.

If it is assumed that the source can be represented by a horizontally propagating unilateral rupture, then the 'directivity' effect is described by the expression proposed by *Ben-Menahem* [1961], introducing variable X,

$$X = \frac{1}{2}\frac{\omega L}{C}\left(\frac{C}{v} - \cos\theta\right)$$

where L is the fault length, C is phase velocity, v is velocity of rupture propagation, and θ is the angle between the direction of rupture propagation and direction to the receiver. The correction to the spectrum, F_p, computed for a point source is then

TABLE 5. Comparison of Moment Tensor for a Deep Earthquake, the Honshu Event of March 7, 1978

		Principal Axes of Moment Tensor					
		Tension Axis		'Null Axis'		Compression Axis	
	Scale Factor, dyn cm	Value	Plunge/ Azimuth	Value	Plunge/ Azimuth	Value	Plunge/ Azimuth
Our result (SRO and ASRO data)	10^{26}	3.9	52/66	0.2	0/157	−4.1	37/247
Result of Masters and Gilbert (IDA data)	10^{26}	5.2	49/40	0.0	25/161	−5.2	31/267

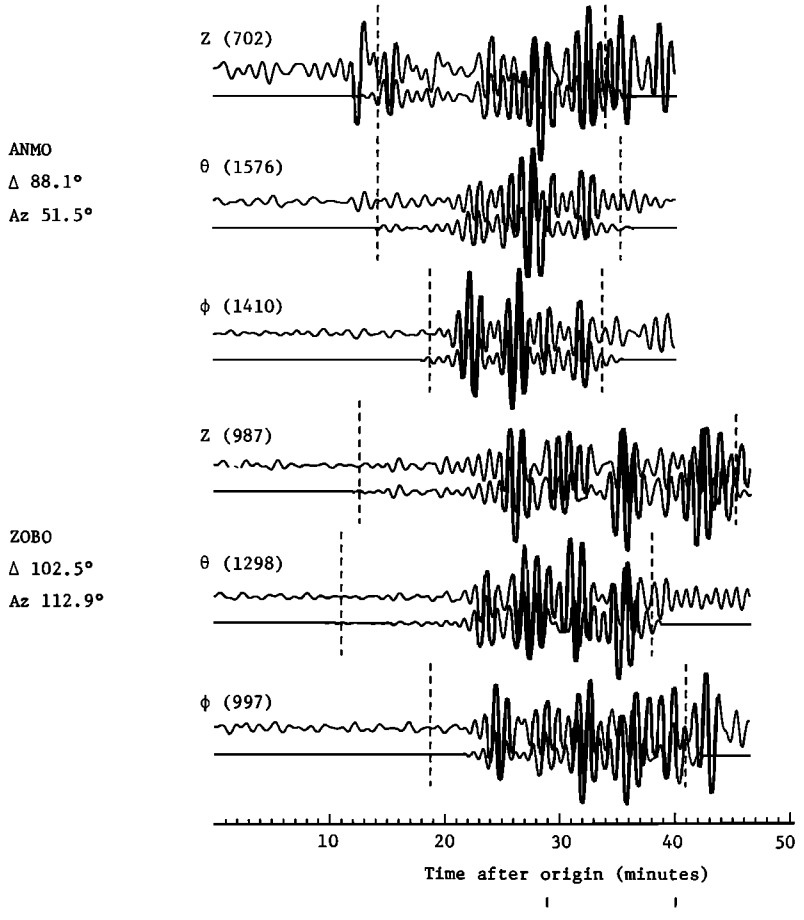

Fig. 5*a*. Comparison of the observed and synthetic seismograms for stations ANMO and ZOBO for a deep (600 km) event of April 24, 1979 (event 10 in Table 4). The top trace for each pair represents the observed seismogram; the bottom trace is the synthetic computed for the source mechanism obtained by the iterative inversion of the data from 12 SRO/ASRO stations. The scale is common for each pair of traces. The numerical factor corresponds to the maximum amplitude for a given pair of traces. It represents the digital count of the SRO instruments; the ASRO response has been appropriately normalized. Only the data between the vertical broken lines were used in the analysis. Notice the glitch associated with the *P*-wave arrival on the vertical component of station ANMO. This is a rather distant station ($\Delta = 88°$) and the only one that exhibited the nonlinear behavior, even though station SNZO is only 21° from the epicenter. This unpredictability of the nonlinear response of the SRO stations is both puzzling and worrisome.

$$F(\omega) = F_p(\omega)e^{-iX} \cdot \sin X/X$$

It is the ratio of C/v that determines the relative importance of the directivity effect with respect to that of the finite duration: if $C/v \sim 1$, then the directivity can be important, depending on the magnitude of the product of frequency and source duration. If $C/v \gg 1$, then it is sufficient to consider only the source duration. Assuming that the average phase velocity of the waves used in our analysis is 10 km/s, then $C/v \sim 3$, and the source duration effect is much more important than the directivity effect. We searched for a source duration T that minimizes the rms error. For this particular earthquake we found the optimal T to be 24 s. It is not an unreasonable value for an earthquake with a magnitude greater than 7: the maximum eigenvalue is 8.7×10^{26} dyn cm.

The change in epicentral position is roughly 70 km to the east; the change in depth is small: only 8 km. Because of the narrow band nature of our data it is difficult to make definite statements with respect to the faulting history. The relatively large value of ϵ (0.18) may be indicative of the complexity of faulting geometry. Undoubtedly, analysis of the IDA data for this earthquake should be very helpful, as it was certainly large enough to excite a rich normal mode spectrum.

3. Analysis of a Foreshock and Aftershocks of the Sumba Earthquake of August 19, 1977

This earthquake (ISC origin time and location: 0608:54.8, latitude 11.16°S, longitude 118.41°E, depth determined from *pP-P* intervals, 78 km) was one of the largest events since the Alaskan shock of 1964. For the first time in 13 years the modes ${}_0S_2$ and ${}_0S_3$ were detected, and, because of the improved coverage with high-quality instruments of the IDA network, their multiplet structure has been completely resolved [*Buland et al.*, 1979]. The current estimate of the seismic moment of this earthquake is 5×10^{28} dyn cm (H. Kanamori, personal communication, 1980), nearly 2 orders of magnitude greater than the largest event analyzed in this report. The instruments of the SRO and IDA networks were saturated for several hours, and obviously, our method of analysis could not be applied to the main event. However, detailed studies of the mechanism of earthquakes preceding and following a major event are equally, if not more, important, as they yield information on the pattern of redistribution of stress in a particular region. This is the stage at which the ability to obtain precise quantitative evaluation of moderate size earthquakes is important.

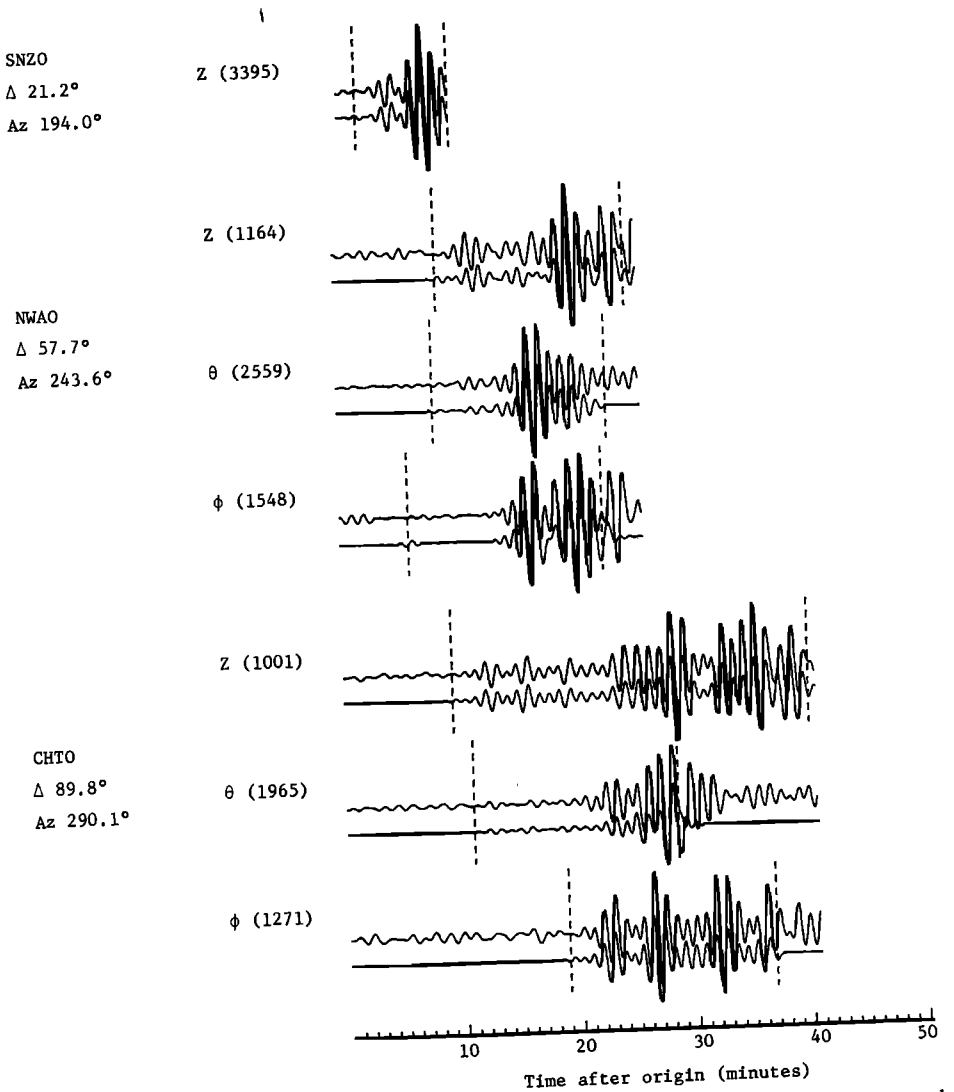

Fig. 5*b*. Same as Figure 5*a* but for stations SNZO, NWAO, and CHTO. Notice the perfect agreement between the observed and synthetic traces for the vertical component at station SNZO. The excellent agreement between the observed and synthetic seismograms is commonly achieved for stations close to the epicenter or for the early parts of recordings at distant stations.

In this report we present results for five earthquakes in the immediate vicinity of the main shock, and six events at some distance from the main fault which, we believe, are associated with the process of stress redistribution.

The SRO/ASRO network was not yet fully operational in August 1977; the number of stations used in the analysis ranged from 5 to 8, as opposed to the 15 stations used to study event 6 (section 2*d*5) of September 15, 1978, for example. Consequently, the results have larger standard errors, and our determinations of the epicentral locations must be considered with caution, as the inadequate azimuthal coverage makes this experiment particularly vulnerable to errors in location along the east-west axis. In Figure 7 we show distribution of the SRO/ASRO stations that were operational during the period from August 19, 1977, to October 16, 1977; the projection is centered on the epicenter of the main event. Unfortunately, data from only a part of the network were available for analyses of individual events.

The map in Figure 8 shows the distribution of the events in the vicinity of the main shock, designated by a large triangle. Dots indicate the ISC locations, stars are our relocations. The foreshock, according to the ISC, is within a few kilometers of the main event and occurred about 1 hour before it. There were six stations available for the analysis of this earthquake. Our solution (Table 6) is consistent with the normal faulting mechanism determined for the main event by *Stewart* [1978]. The slight clockwise rotation of the strike (~15°) with respect to the axis of the trench need not be significant. Our estimate of the hypocentral depth represents a 16-km decrease from the value reported by the ISC; this is a very systematic effect: in all cases in which the hypocentral depth was allowed to vary, we obtained depths shallower by 10 to 20 km. *Fitch et al.* [1981], from their analysis of the surface reflected body wave phases, infer even shallower depths for most of these events. However, fixing the depth of the foreshock at 16 km does not cause any essential change in our solution. The intermediate eigenvalue is relatively large: $\epsilon = 0.23$. It is interesting to note that two aftershocks also yielded substantial values of ϵ (0.17 and 0.14); in all three cases the maximum eigenvalue was associated with compression; for the remaining two aftershocks

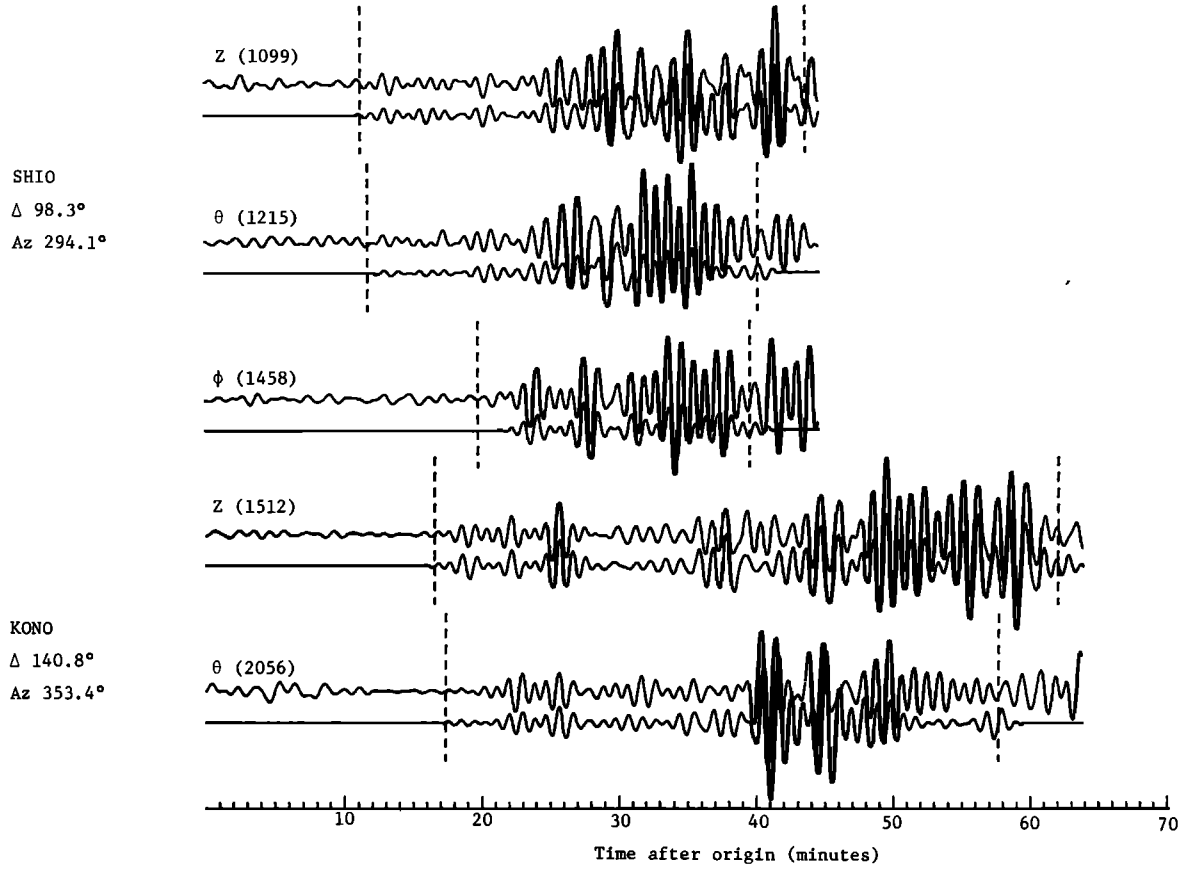

Fig. 5c. Same as Figure 5a but for stations SHIO and KONO. Notice that for the vertical component traces at station KONO the observed and synthetic seismogram agree in all important details for the entire 45-min-long interval. At the same time, the synthetic traces for the longitudinal component show systematically too low amplitudes. This effect is very common, and we believe that it reflects an important difference between our reference earth model and the real earth. We think that this difference is associated with a rather shallow feature of the structure.

the value of ϵ was essentially zero. In the graphical representation of the source mechanism (bottom of Figure 8) we treat the axis associated with the intermediate eigenvalue as if it were the null axis; that is, we plot only the solutions for the 'major double couple,' in the terminology of section 2*d*5.

The first of the four analyzed aftershocks occurred roughly 3 hours after the main event and appears to have essentially the same mechanism as the foreshock and the main shock. Two aftershocks that occurred on the 25th and 26th of August are located some 80 km to the east, relatively close to the place where the axis of the Java trench changes its direction; it may be that these two solutions (both with appreciable values of ϵ) are affected by this feature. Although normal faulting is the dominant component for all four earthquakes discussed so far, there is some asymmetry: the nodal plane dipping in essentially a northerly direction has a dip angle between 55° and 62°; the dip of the second nodal plane ranges from 34° to 25°.

The event on September 23 has a distinctly different source mechanism: the normal faulting component, which has the same sense as all other events discussed so far, is slightly exceeded by the dip-slip component of opposite direction than for earlier events; the strike direction (287°) remains predominantly east-west. The fact that this aftershock is to the west of the main event and that it occurred over 1 month later may be responsible for its distinctly different mechanism. The moments of the analyzed events ranged from 8×10^{24} to 5×10^{25} dyn cm.

Substantial seismic activity began in an area some 150 km to the northwest of the main event nearly 50 days later; some of the largest events occurred on October 7, 1977. We have selected five of these events; in addition, we have also analyzed an earthquake on October 16 that occurred in the same area. The area of seismicity is in the center of Figure 9 and the major double-couple nodal plane solutions are shown at the top of that figure. The numerical results are given in Table 7.

There could be some question whether this sequence of earthquakes is related to the August 19 event; we do not think that a direct proof is possible. However, if we consider the fact that the seismicity in this particular area has been generally low, there is a strong indication that these two occurrences are related. The source mechanism of these events also seems to suggest that this is the case.

All five earthquakes on October 7 are nearly perfect strike-slip events with the average azimuth of the compression axis of 167° (347°) and 77° (257°) for the axis of tension; the azimuths of the nodal planes are thus 32° or 122°. The latter one agrees well with the axis of the aftershock zone and points towards the main shock area. If this is the plane of slip, then it is right-lateral. This is the sense of motion that one would expect from redistribution of the stress in the region due to the change in strain associated with the main shock.

In Table 8 we indicate which of the stations of the network were available for the analysis of the events listed in Tables 6 and 7. Most of the differences among the relocation vectors may be associated with a change in station coverage.

For the given distance from the main shock (~150 km) the time at which these events occurred could be compared with calculations of *Melosh* [1976] for stress propagation in the asthenosphere of nonlinear rheology. Using his Figure 8, we find that the point corresponding to a time of 50 days falls between the curves for $n = 2$ and $n = 3$, where n is the exponent in the expression for the strain rate [see *Melosh*, 1976, equation (1)]. It is certainly interesting that this is the same range of values as inferred by Melosh for the aftershock sequence following the Rat Island earthquake of February 4, 1965.

4. Discussion and Conclusions

In the introduction we stated several objectives that should be met by a method of quantitative analysis of the data from a global digital seismograph network. We think that the examples of application shown in this paper demonstrate that the approach proposed by us does indeed satisfy these requirements.

The time window and the frequency band chosen for the analysis lead to repeatable solutions for the moment tensor even when there is a marked disagreement between the observed and synthetic seismograms for a significant part of the total data set used in inversion.

This is an important result. It implies that the discrepancies between the kernel functions and observed seismograms for late times at distant stations have the character of random noise. Inclusion of this noise in the analysis is unable to alter substantially the solution obtained from the part of recording for which we obtain a high degree of coherence between the data and the synthetics. It is unclear how little data must be included in the analysis in order to obtain a reliable solution for the source mechanism and location of an earthquake. The answer must depend on distribution of receivers, hypocentral depth, and source mechanism, which is not known a priori. What is essential, however, is that the robustness of the procedure provides us with a 'bootstrap' that could be used in the future to incorporate in the analysis inversion for the earth's structure.

An earth model obtained by inversion of a large body of reliable seismological data, such as model 1066B used throughout this study, is bound to match well the early part of observed traces; the level of agreement at late times and large distances depends strongly on the source depth. For very deep earthquakes the agreement is generally excellent, as the waveforms are weaker functionals of the upper mantle structure. The disagreement at late times may be related in part to the effect of lateral heterogeneities and in part to discrepancies

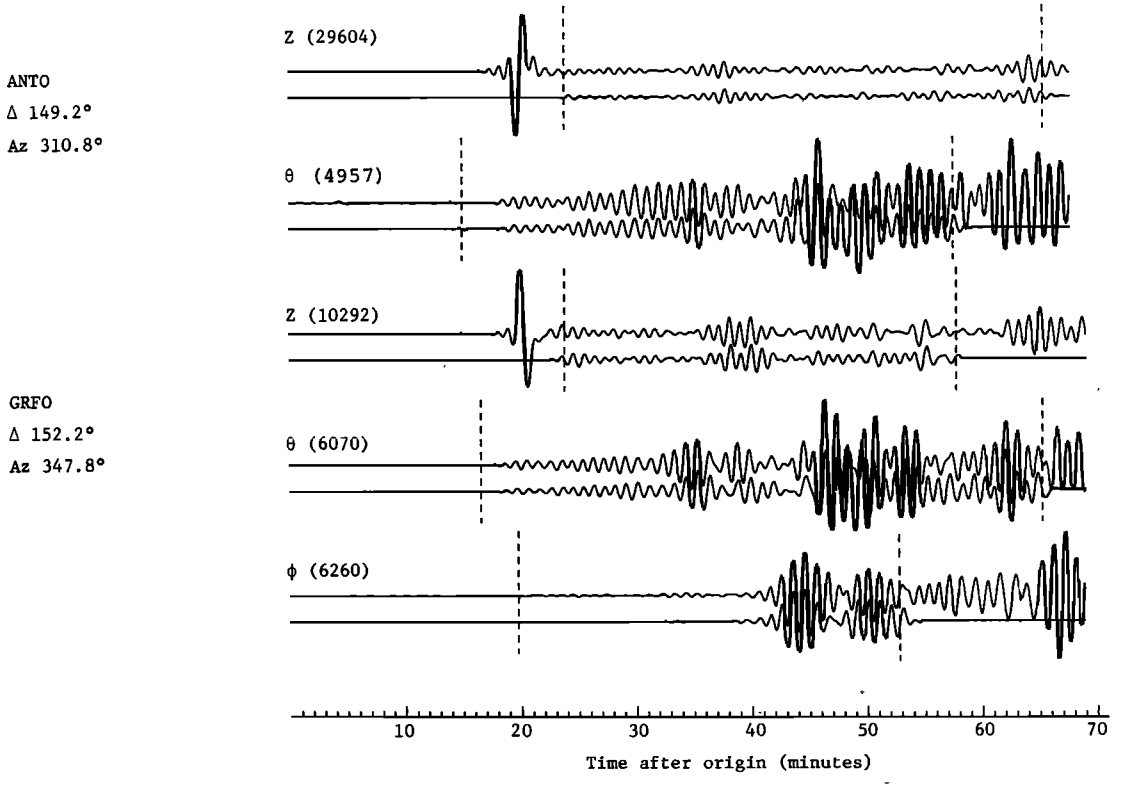

Fig. 6. Comparison of observed and synthetic seismograms for stations ANTO and GRFO for an intermediate depth earthquake of August 5, 1979 (event 13 in Table 4). The top trace for each pair represents the observed seismogram; the bottom trace is the synthetic computed by the iterative solution. For additional details, see the caption to Figure 4*a*. Our source mechanism for this event shows a particularly large deviation from a simple double-couple mechanism. The agreement between the observed and synthetic seismograms is very good; at these large distances ($\Delta \sim 150°$) the traces contain significant contributions from waves traveling along the major arc. Notice that even for PKP waves the SRO stations exhibit nonlinear response.

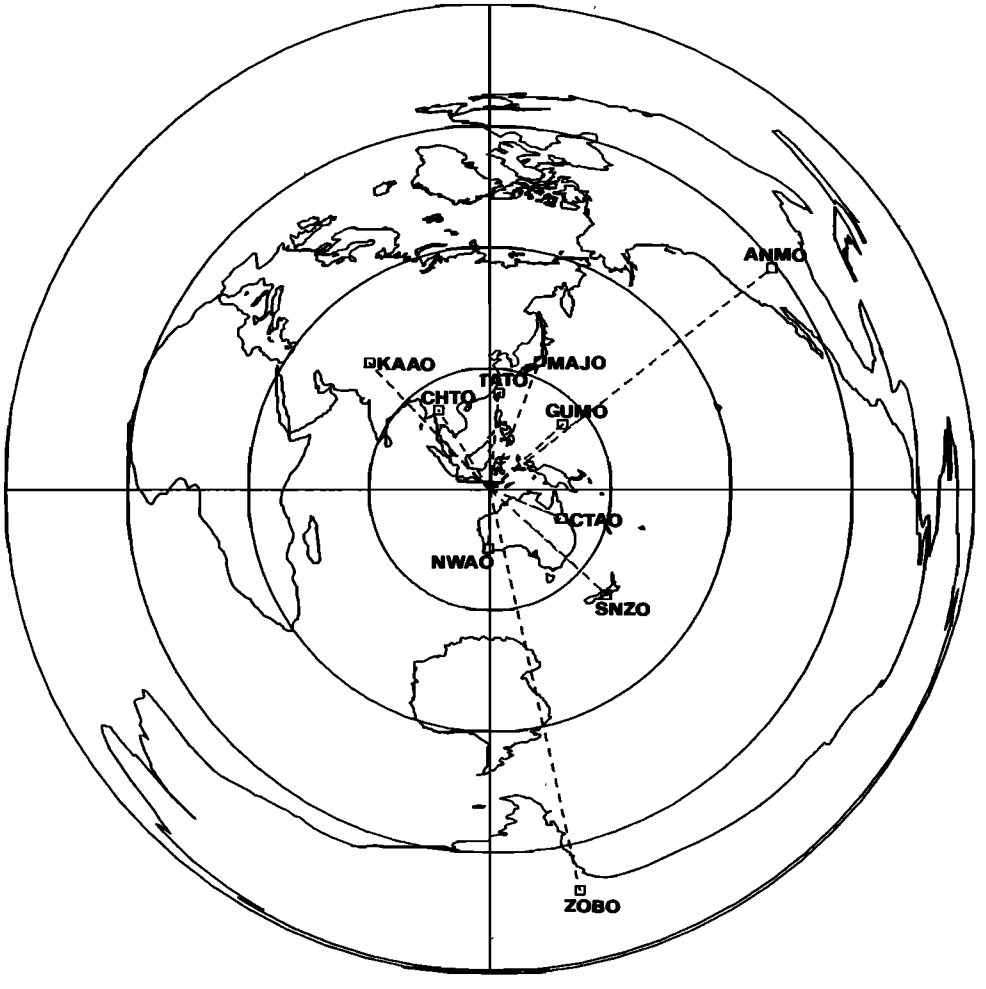

Fig. 7. Equidistant projection centered on the location of the main shock of the August 19, 1977, Sumba earthquake showing the distribution of the SRO/ASRO stations operational from August to October 1977. However, only a fraction of the network was available for the analysis of individual earthquakes. The details are given in Tables 6, 7, and 8 and Figures 8 and 9.

between the reference earth model and the optimal 'average earth' structure. Systematically too small amplitudes predicted for the longitudinal component at late times and large distances indicate that this may be the case.

In section 2*d*2 we have pointed out that the excitation kernels depend on the earth structure in two different ways: through the eigenfunctions of normal modes as well as through their eigenvalues. Perturbations in eigenvalues can be linearly related to small changes in the elastic and anelastic parameters of the earth structure. Thus the inverse problem could be expanded to incorporate, in addition to inversion for the properties of the source, also the search for perturbations in the structural parameters. Data for many earthquakes could be processed at the same time, and eventually, the problem of large scale lateral heterogeneities could also be approached along these lines. The viability of this scheme depends on the answer to the question of whether convergence can be initiated using the eigenfunctions predicted by the starting model. This question could be answered by performing appropriate numerical experiments. If the answer is favorable, then the project is entirely feasible; if not, an alternative approach will have to be developed. Our results demonstrate that we have an adequate starting model for the earth structure as well as a stable initial solution for the source mechanism.

The seismic moments of the events analyzed in this report ranged from 5×10^{24} to 8×10^{26} dyn cm. The lower range could be extended by incorporating higher frequencies in the analysis, although this would increase markedly the required expenditure of computer time.

The other possibility is to calibrate the phase velocity dispersion and apparent attenuation of the fundamental model surface waves for a particular source-receiver path using the moment tensor obtained by the method described in this paper. These two functions of frequency can then be used for studies of source mechanism of other earthquakes in the vicinity of the calibration event. This would extend the magnitude range, allowing for studies of events with moments substantially smaller than 5×10^{24} dyn cm, and also significantly reduce the time required for the analysis. The most difficult part of studying the earthquake mechanism from the signal of the fundamental mode alone is the separation of the effect of lateral heterogeneities [*Patton*, 1978; *Aki and Patton*, 1978]. Of course, application of the calibration events in the manner described above can be, by itself, a valuable tool in studying the laterally heterogeneous structure of the crust and upper mantle.

The dynamic range of SRO instruments is too small to allow the analysis of the early parts of the recordings of events with moments exceeding 5×10^{27} dyn cm. These can be studied us-

ing truncated records sometimes beginning hours after the origin time [*Dziewonski and Gilbert,* 1974; *Masters and Gilbert,* 1979; *Kanamori,* 1980], but the loss of information on the properties of the source spectrum at periods below, say, 100 s, is irreversible. We hope that the response of the digital WWSSN stations will meet to some degree the recommendations of the Panel on Global Seismograph Networks [*Engdahl,* 1977] with respect to the need for on-scale recording.

The approach to evaluation of excitation and location kernels by summation of normal modes eliminates the need for identification and separation of individual phases to be used in inversion for the moment tensor. Although the method would clearly be impractical if the period range of the analysis were to be extended below 10 s, the effect of lateral heterogeneities imposes a natural short-period limit for our approach to the problem. Considering the fact that the S-wave station anomalies can be as large as several seconds [*Hales and Doyle,* 1967] and a similar range of variability is observed for the travel times of nearly vertical reflections [*Sipkin and Jordan,* 1975, 1976, 1980; *Okal and Anderson,* 1975], extension of the frequency range much below 30 s does not appear desirable, unless some system of corrections could be devised.

If it were not for the glitches, erroneous multiplexing, and reversal of the polarities of components in the data from the SRO/ASRO network, the analysis could be completely automated. As it is, multiple visual examination of the records is required, and this is, by far, the most time-consuming part of the entire process.

The requirements of computer time needed for the analysis are moderate but strongly depend on the choice between limiting the analysis to the initial iteration (finding components of the moment tensor for a given set of the hypocentral parameters) or application of the iterative scheme, in which the search for the best position of the stress glut centroid is made.

If in future routine operations only inversion for the moment tensor were to be performed, then it would be advisable to store a library of functions σ_{ij} (see the appendix, equation (A15)) computed at intervals of, say, 10 km, for a depth range from 0 to 700 km. Deviation of any particular source depth from the closest entry in the library would not be greater than

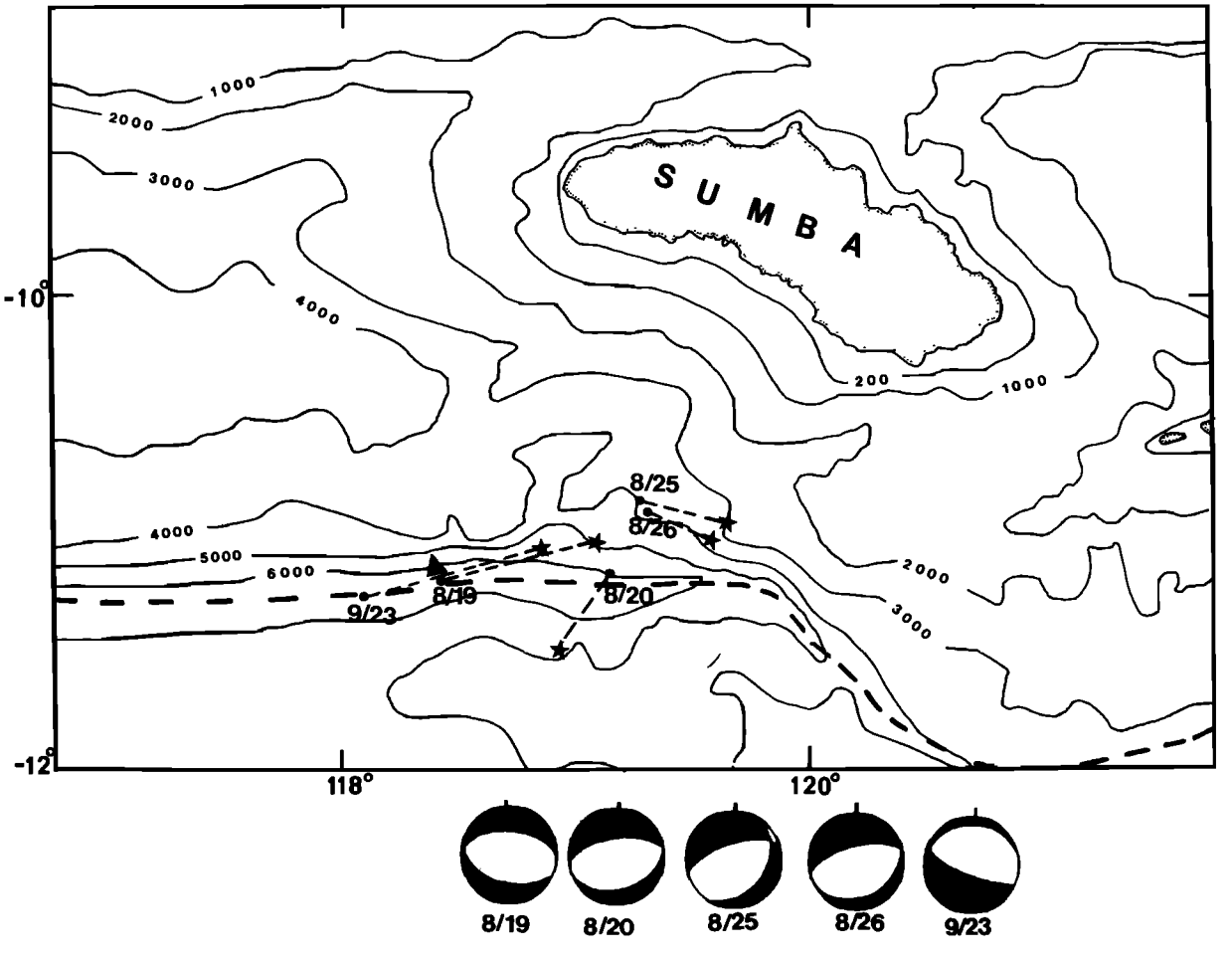

Fig. 8. The bathymetric map of the seafloor in the vicinity of the main shock of the August 19, 1977, Sumba earthquake, shown by the large triangle. The axis of the Java trench is shown by the long-dashed line. The dots accompanied by dates designate the ISC locations of the foreshock (August 19 (8/19)) and four aftershocks studied by us. The stars show our relocations of these events. The number of available stations was small at the time of the Sumba event, and the results of relocation should be treated with caution. The aftershock of August 20 shows a direction of relocation significantly different from those of the other four events; there were only 5 stations available to analyze this event, and its relocation is particularly doubtful. The nodal plane solutions are shown at the bottom of the figure; dark areas designate the part of the focal sphere where compressional first arrivals would be expected in a first-motion study. In plotting these nodal plane solutions we have ignored deviations from the pure double-couple mechanism. Our solutions indicate that the dominant feature of the aftershock series was normal faulting along the trench axis.

TABLE 6. Results of Inversion for the Moment Tensor and Hypocentral Parameters of a Foreshock and Four Aftershocks of the Sumba Earthquake of August 19, 1977

	Event A1, Aug. 19, 1977	Event A2, Aug. 20, 1977	Event A3, Aug. 25, 1977	Event A4, Aug. 26, 1977	Event A5, Sept. 23, 1977
			ISC		
Origin time	0508:43.6	0921:50.5	1805:11.9	0826:36.5	0557:55.8
Latitude	11.21°S	11.19°S	10.88°S	10.92°S	11.29°S
Longitude	118.43°E	119.14°E	119.26°E	119.30°E	118.10°E
Depth,* km	54	33	51	33	34
			Our Results		
δt_0, s	4.3 ± 0.4	7.7 ± 0.3	5.4 ± 0.3	5.1 ± 0.4	8.0 ± 0.5
Latitude	11.06°S ± 0.04	11.07°S ± 0.04	11.02°S ± 0.03	11.23°S ± 0.04	11.08°S ± 0.05
Longitude	119.08°E ± 0.05	119.06°E ± 0.05	119.63°E ± 0.03	119.57°E ± 0.04	118.83°E ± 0.07
Depth,* km	38 ± 2.3	33	31 ± 1.7	33	24 ± 1.8
Scale Factor, dyn cm	10^{25}	10^{25}	10^{25}	10^{25}	10^{24}
			Moment Tensor		
f_1	−1.07 ± 0.05	−1.54 ± 0.11	−4.17 ± 0.15	−1.18 ± 0.05	−5.05 ± 0.19
f_2	0.77 ± 0.04	1.54 ± 0.11	2.33 ± 0.14	0.91 ± 0.05	5.04 ± 0.25
f_3	0.30 ± 0.04	0.00 ± 0.11	1.84 ± 0.19	0.27 ± 0.06	0.01 ± 0.30
f_4	0.36 ± 0.06	0.73 ± 0.18	2.55 ± 0.29	0.70 ± 0.09	−6.01 ± 0.87
f_5	0.01 ± 0.06	0.13 ± 0.17	0.18 ± 0.22	0.14 ± 0.07	2.18 ± 0.91
f_6	−0.16 ± 0.04	0.40 ± 0.09	1.55 ± 0.13	0.24 ± 0.04	−1.10 ± 0.18
			Principal Axes		
T axis					
Moment	0.88	1.80	4.20	1.20	8.29
Plunge/azimuth	10/15	12/347	15/326	17/343	26/195
N axis					
Moment	0.26	−0.09	0.87	0.20	−0.15
Plunge/azimuth	4/285	1/77	13/59	2/74	4/287
P axis					
Moment	−1.14	−1.71	−5.07	−1.40	−8.14
Plunge/azimuth	79/171	77/173	70/188	73/172	64/26
Stations used	5	5	6	6	7

*Depth has been fixed at 33 km for the first and third aftershocks.

5 km, which seems quite acceptable, considering that the usual uncertainty in the hypocentral depth is at least of that order. With an established library of functions σ_{ij} and a network of, say, 15 three-component stations, evaluation of the excitation kernels and formation of the inner product matrix and its inverse take less than 10 min on an Interdata 8/32 computer or approximately 5 min on a faster processor such as VAX780.

If the relocation procedure is required, then the execution time is substantially greater, as the functions σ_{ij} must be recomputed following each iteration. For the same network of 15 stations the time required per iteration is approximately 20–25 min, or typically, 70–100 min per solution. This is still not prohibitive, considering the limited number of earthquakes that would be analyzed in that mode.

In this paper we have analyzed 25 events, 11 of which were related to the Sumba earthquake of August 19, 1977, and most of the remaining 14 were located in the seismic zones of the western and southern Pacific, except for two earthquakes in South America and one near the triple junction in the South Atlantic.

For the set of 14 earthquakes our solutions for the moment tensor are highly consistent with those obtained by other researchers using different methods and data sources (nodal plane solutions, inversion for the moment tensor using ultra-long-period data from the IDA network). In this sense, there were no surprises, but rather we have demonstrated that our approach gives reliable solutions even at shallow depths, at which inversions based on ultra-long-period data encounter difficulties with resolution of the $M_{r\theta}$ and $M_{r\phi}$ components.

Our most important finding with respect to the nature of source mechanisms is that a substantial number of earthquakes of intermediate and great depth have significant non-double-couple components. Of 11 events in this depth range, 5 have substantial values of ϵ ($\epsilon = |\lambda_{min}/\lambda_{max}|$) ranging from 0.16 to 0.28, and for 6, ϵ is very small; from 0 to 0.05. Admittedly the population is small, but the indication is that the frequency of deviation from the double-couple mechanism is quite high. It would be most interesting to increase the data base and investigate whether there is consistency among earthquakes in the same seismic zone and depth range. The only pair of earthquakes in the immediate vicinity of each other (events 5 and 7) available in this study yielded nearly identical solutions, and in both cases, ϵ was zero (pure double couple).

At the same time, nearly all shallow earthquakes yielded essentially pure double-couple solutions. The results for the foreshock and aftershocks of the Sumba earthquake must be considered less reliable because of the paucity of station coverage.

The novel element of this study has been the expansion of the inverse problem to include perturbations in the hypocentral parameters. Ideally, we would like to distinguish between the location and time of the initiation of rupture and the cen-

troid of the stress glut; such information would be invaluable in studies on the nature of earthquakes, particularly at depths and locations that make other methods of estimating the source dimension inapplicable.

Unfortunately, the absolute locations obtained by the analysis of the arrival times of *P*-waves have uncertainty that may reach several tens of kilometers, and our procedure shows on occasion changes in location that seem excessive and, in case of poor station coverage, very sensitive to the particular distribution of receivers. Thus at this stage, the results are of a purely exploratory nature. However, two of the parameters that are determined by the inverse procedure seem to yield reliable and useful information even now.

Hypocentral depth. The energy radiated upward from the source and reflected from the surface is approximately equal to that radiated downward. Thus our excitation kernels are highly sensitive to the source depth, as they contain the complete suite of the depth phases. On the basis of comparison with the standard depth determinations we infer that our solutions are reliable. In instances of a major revision in depth estimates between the PDE and monthly bulletins issued by the NEIS, our results show better agreement with the improved estimate, even if we use the PDE parameters as the starting location. With few exceptions, our results show a systematic shift towards shallower depths; this is particularly apparent for the shallow earthquakes. Thus the ability of the method to provide an objective depth determination should be considered one of its most important immediately applicable features. There is no reason to think that the depth determination would be potentially as sensitive to the influence of lateral heterogeneities as the epicentral coordinates and, perhaps, the origin time might be.

Origin time. Perturbations in the origin time, δt_0, are positive for all events analyzed in this report, thus indicating the finite duration of the analyzed sources. There is an overall increase of δt_0 with the increase in the moment, as should be expected. However, a major change in the hypocentral depth obviously affects the estimate of the origin time; for this reason, without introducing corrections for this effect, we cannot test the direct relationship between the source duration (L/v, for unilateral faulting) and the change in the origin time. Without a change in depth and in the absence of a significant base line correction, one could assume that the source duration equals $2\delta t_0$. In general, the figures obtained in this way

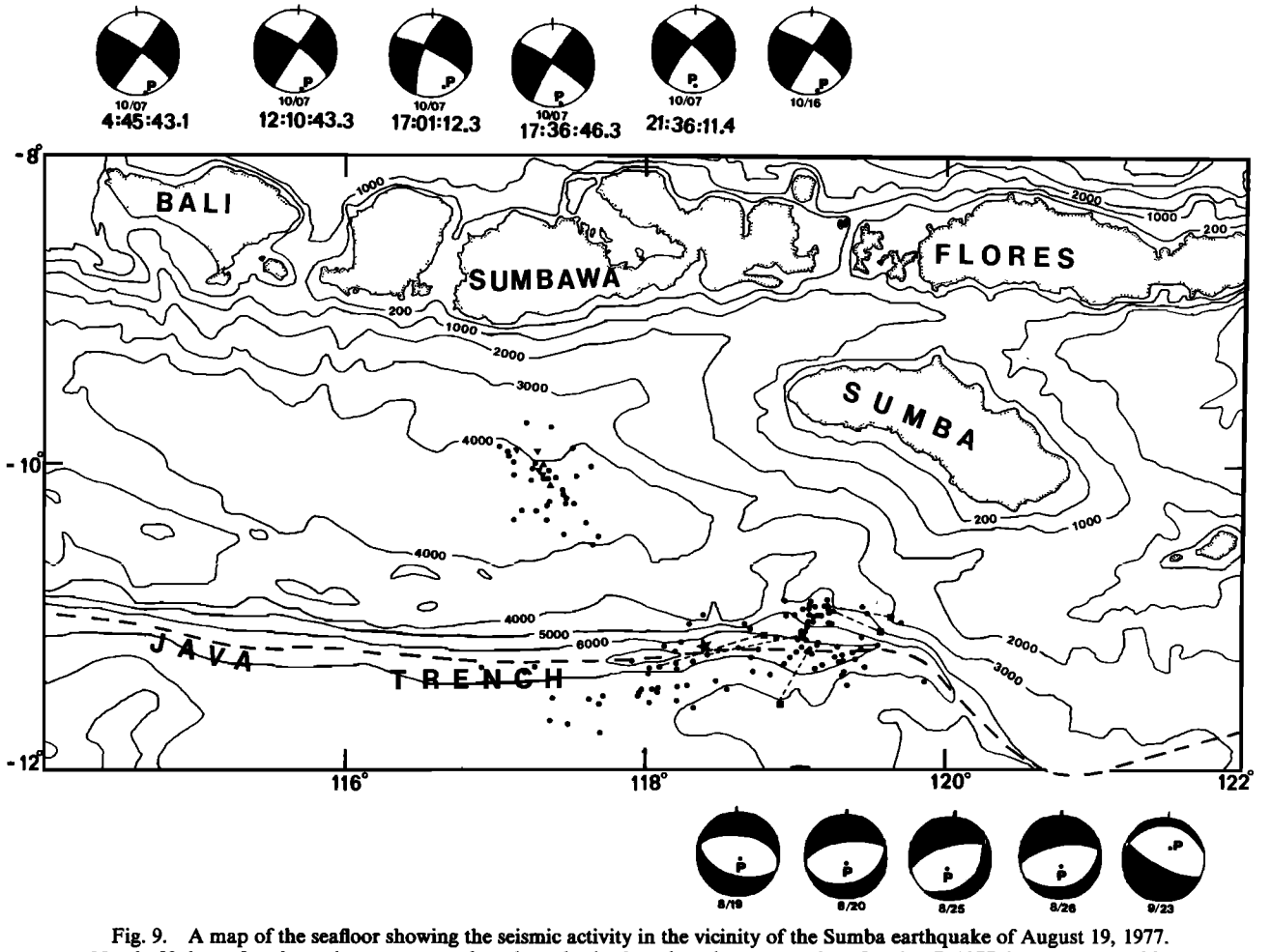

Fig. 9. A map of the seafloor showing the seismic activity in the vicinity of the Sumba earthquake of August 19, 1977. Nearly 50 days after the main event, several moderately sized earthquakes occurred on October 7, 1977, in an area roughly 150 km to the northwest of the main event shown by the star. Our analysis of five earthquakes of October 7 shows that their mechanism was strike slip faulting (see the top of the figure) with one of the nodal planes pointing towards the main event. If this is the plane on which the slip took place, the motion would be right-lateral. This mechanism is consistent with a concept of regional readjustment of stress following a major earthquake. For comparison, our solutions for the events in the immediate vicinity of the main shock are added at the bottom of the figure.

TABLE 7. Results of Inversion for the Moment Tensor and Hypocentral Parameters of Six Earthquakes South of the Sumbawa Island That Occurred on October 7, 1977

	Event B1, Oct. 7, 1977	Event B2, Oct. 7, 1977	Event B3, Oct. 7, 1977	Event B4, Oct. 7, 1977	Event B5, Oct. 7, 1977	Event B6, Oct. 16, 1977
Origin time	0445:43.1	1210:43.3	1701:12.3	1736:46.3	2136:11.4	2109:18.2
Latitude	10.07°S	9.99°S	9.92°S	9.83°S	9.97°S	9.83°S
Longitude	117.35°E	117.29°E	117.30°E	117.26°E	117.27°E	117.11°E
Depth,* km	30	29	27	31	36	39
			Our Results			
δt_0, s	3.7 ± 0.4	4.9 ± 0.3	4.2 ± 0.5	3.5 ± 0.5	4.4 ± 0.5	7.0 ± 0.3
Latitude	10.13 °S ± 0.04	10.01°S ± 0.03	9.68°S ± 0.04	9.98°S ± 0.07	9.93°S ±0.05	9.76°S ± 0.03
Longitude	117.54°E ± 0.08	117.62°E ± 0.05	117.06°E ± 0.07	117.52°E ± 0.12	117.64°E ± 0.07	117.64°E ± 0.05
Depth,* km	(20)	(20)	(20)	(20)	(20)	(20)
Scale factor, dyn cm	10^{24}	10^{25}	10^{24}	10^{24}	10^{24}	10^{25}
			Moment Tensor			
f_1	0.61 ± 0.30	0.24 ± 0.09	−1.01 ± 0.21	1.48 ± 0.31	−1.71 ± 0.17	0.25 ± 0.04
f_2	−8.00 ± 0.34	−3.89 ± 0.13	−6.65 ± 0.29	−6.83 ± 0.50	−2.90 ± 0.28	−1.89 ± 0.06
f_3	7.39 ± 0.46	3.64 ± 0.16	7.66 ± 0.35	5.35 ± 0.59	4.61 ± 0.29	1.65 ± 0.07
f_4	0.61 ± 0.64	0.69 ± 0.24	2.07 ± 0.36	1.19 ± 1.03	1.84 ± 0.49	0.49 ± 0.08
f_5	1.25 ± 0.50	0.67 ± 0.14	−0.60 ± 0.40	0.15 ± 0.60	0.05 ± 0.36	0.10 ± 0.06
f_6	−2.05 ± 0.38	−2.10 ± 0.10	−1.32 ± 0.23	3.44 ± 0.36	−4.25 ± 0.21	−0.15 ± 0.05
			Principal Axes			
T axis						
Moment	7.85	4.24	7.85	6.26	6.59	1.66
Plunge/azimuth	9/263	7/256	5/84	2/75	5/65	3/268
N axis						
Moment	0.49	0.33	−0.45	1.63	−1.01	0.35
Plunge/azimuth	80/54	78/20	72/338	82/330	65/324	77/13
P axis						
Moment	−8.34	−4.57	−7.40	−7.89	−5.58	−2.01
Plunge/azimuth	5/172	10/165	18/176	7/165	24/157	12/177
Station used	7	7	8	6	7	8

* Depth has been fixed at 20 km and not allowed to change in inversion.

are not unreasonable, and they are essentially consistent with the relationship $L \sim M_0^{1/3}$ [*Kanamori and Anderson,* 1975]. We feel that at this time we have too few data points to attempt the quantitative analysis of the dependence of the source duration on the seismic moment.

The sensitivity of our method to perturbations in the origin time is quite high, even at the relatively long periods used in this study. The kernel for δt_0 is proportional to the time derivative of the synthetic seismogram obtained for the parameters from the previous iteration (equation (3)). Assuming that the dominant frequency is 0.1 radian/s (period of 62.8 s), a 1-s perturbation in δt_0 leads to a 10% change in the relative rms error.

TABLE 8. Stations Available for Inversion for the Moment Tensor and Hypocentral Parameters of Earthquakes in Tables 6 and 7

Station	Event										
	A1	A2	A3	A4	A5	B1	B2	B3	B4	B5	B6
ANMO					X		X	X	X		X
CTAO	X	X	X	X	X	X	X	X		X	X
SNZO	X	X	X	X	X	X	X	X	X	X	X
ZOBO					X	X	X	X		X	X
NWAO		X				X		X	X	X	X
KAAO	X	X	X	X	X	X	X	X	X		
CHTO	X	X	X	X	X					X	X
TATO	X		X	X	X	X	X	X	X	X	X
MAJO			X	X							
GUMO						X	X	X	X	X	X

X indicates that a particular station was used for a given event.

In this study we have used an earth model that was derived before the frequency dependence of the elastic parameters due to anelastic attentuation was widely recognized [cf. *Liu et al.*, 1976]. In the future it will be desirable to use a model in which this effect is considered, as this may affect the estimates of δt_0. In terms of this report, application of the model 1066B, derived by inversion of free oscillation data, should have resulted in a negative contribution to δt_0: the model can be expected to be 'slower' at a period of 60 s than the real earth.

Epicentral coordinates. This is perhaps the most uncertain aspect of our results. In some cases the perturbation with respect to the standard locations is very small; for event 10 it was approximately 6 km. It is also reasonable (~20 km) for two other deep events (3 and 11). However, for several shallow earthquakes it appears to be excessive: see event 6, in particular.

The relative locations seem to be more consistent. Two close intermediate depth events (5 and 7) show very similar perturbations in their location. The foreshock and aftershocks of the Sumba earthquake show similar shifts in the epicentral coordinates as long as the station coverage is consistent; see Figure 8. The aftershock on August 20 (event A2) has, however, a distinctly different relocation vector, because of change in the network pattern, as indicated in Table 7. The reason for the significantly different relocation vector for event B3 is not entirely clear, as the change in the network coverage is not as striking.

We expect that the effect of lateral heterogeneities is the main source of error. This, in part, can be compensated for by improved network coverage. The planned deployment of

WWSSN stations with digital recording should be extremely helpful in this respect, particularly in terms of more balanced azimuthal distribution of receivers.

Although we admit that some of our relocations should be considered with caution, we believe that it is very important that the problem be studied further. As the standard locations are not free from systematic errors due to lateral heterogeneities, results obtained using our method offer an opportunity to look at the source through a different filter; the wavelengths used in our study are 1–2 orders of magnitude greater. The effect of lateral heterogeneities associated, for example, with subducted slabs may be different and, perhaps, reduced if one looks at the source with wavelengths of several hundred kilometers.

In the text we have pointed out some flaws in the digital data from the SRO/ASRO network; this should not obscure the fact that the data, on average, are of excellent quality. A major achievement is the superb calibration of the instruments; for example, upon rotation of the horizontal components one obtains a nearly perfect separation of P-SV and SH motions. Also, the agreement between the observed and synthetic seismograms of this study indicates that the global calibration of the network is good.

This research would not have been possible without the high-quality data that the SRO/ASRO network provides. The IDA network is essential for monitoring large-magnitude events; there is a range of overlap between this source of data for ultra long periods and our application of the SRO/ASRO data that is sufficient to establish that we are able to consistently study source mechanisms of earthquakes with moments ranging from 10^{24} to 10^{30} dyn cm. We hope that the global digital seismograph network will be maintained in the future; addition of some 20 WWSSN stations with the digital recording capability would be extremely valuable, as for studies of events of moderate magnitudes there now exists a rather severe imbalance in the geographical distribution of receivers with digital recording.

APPENDIX

In this appendix we give the details of the method of calculation of the synthetic seismograms and their partial derivatives, or kernel functions, with respect to source location and time of occurrence. The simplest derivation of these kernel functions is first to derive the synthetic seismograms due to a source having nonnegligible second spatial and temporal moments; the inverse problem for these second moment tensors would form a natural extension of the work described in this report.

Following *Gilbert* [1971], *Gilbert and Dziewonski* [1975], and *Backus and Mulcahy* [1976], the seismic displacement in a spherically symmetric earth model due to any indigenous source may be written

$$\mathbf{s}(\mathbf{x}, t) = \sum_k \mathbf{S}_k(\mathbf{x}) \int_{-\infty}^{t} dt'' \int_{V_s} d^3x' h_k(t - t') \bar{\mathbf{e}}^{(k)}(\mathbf{x}') : \dot{\mathbf{\Gamma}}(\mathbf{x}', t') \tag{A1}$$

where $\mathbf{S}_k$ are a complete set of eigenfunctions, labeled by the index $k = (n, l, m, q)$—radial order, angular order, azimuthal order, and mode type (q = toroidal or q = spheroidal), respectively. Parameter $\mathbf{e}^{(k)}$ is the strain tensor in the kth mode, and the overbar denotes complex conjugation; $\dot{\mathbf{\Gamma}}$ is the stress glut rate distribution of the source. The time functions $h_k(t)$ are defined by

$$h_k(t) = 1 - \cos \omega_k t \exp(-\tfrac{1}{2} t \omega_k / Q_k) \tag{A2}$$

where Q_k is the quality factor of the kth mode, obtainable from perturbation theory for a given model of attenuation in the earth.

In (A1), $\mathbf{x}$ and $\mathbf{x}'$ are Cartesian coordinates, and the region of spatial integration is over the source region V_s, namely, the region in which $\dot{\Gamma}(\mathbf{x}', t)$ is nonvanishing. *Backus and Mulcahy* [1976] have shown that for modes with wavelengths long in comparison with source dimensions, and periods long in comparison with source duration, (A1) may be usefully expanded in terms of the low-order spatial and temporal moments of the glut rate distribution $\dot{\Gamma}$. Specifically, retaining the first two terms in a Taylor expansion of $\bar{\mathbf{e}}_k(\mathbf{x}')h_k(t - t')$ about a fiducial location $\mathbf{x}' = \mathbf{x}_s$ in the source region and a fiducial time $t' = t_s$ close to the origin time, (A1) becomes

$$\mathbf{s}(\mathbf{x}, t) = \sum_k \mathbf{S}_k(\mathbf{x}) \{h_k(t - t_s)[M_{ij}\bar{e}_{ij}^{(k)}(\mathbf{x}_s) + \Lambda_{ijp}\bar{e}_{ij,p}^{(k)}(\mathbf{x}_s)] - h_k'(t - t_s)H_{ij}\bar{e}_{ij}^{(k)}(\mathbf{x}_s)\} \tag{A3}$$

at times after the source has ceased to act. In (A3), summation over repeated indices is assumed, and the following glut moments have been defined:

$$M_{ij} = \int_{-\infty}^{\infty} dt \int_{V_s} d^3x \dot{\Gamma}_{ij}(\mathbf{x}, t) \tag{A4}$$

$$\Lambda_{ijp} = \Lambda_{ijp}(\mathbf{x}_s) = \int_{-\infty}^{\infty} dt \int_{V_s} d^3x (x_p - x_{sp}) \dot{\Gamma}_{ij}(\mathbf{x}, t) \tag{A5}$$

$$H_{ij} = H_{ij}(t_s) = \int_{-\infty}^{\infty} dt \int_{V_s} d^3x (t - t_s) \dot{\Gamma}_{ij}(\mathbf{x}, t) \tag{A6}$$

The tensor $\mathbf{M}$ is 'the' moment tensor, and $\mathbf{\Lambda}$, $\mathbf{H}$ are the second spatial and temporal moments about $\mathbf{x}_s$, t_s.

Following *Backus* [1977], we define the centroid location $\mathbf{x}_c$ and the centroid time t_c as the values of $\mathbf{x}_s$, t_s for which $\mathbf{\Lambda}$, $\mathbf{H}$ are minimized in the sense that $\Lambda_{ijp}\Lambda_{ijp}$, $H_{ij}H_{ij}$ attain their smallest values. The second moment tensors relative to the centroid will be denoted by

$$\tilde{\Lambda}_{ijp} = \Lambda_{ijp}(\mathbf{x}_c) \tag{A7}$$

$$\tilde{H}_{ij} = H_{ij}(t_c) \tag{A8}$$

and (A3) becomes

$$\mathbf{s}(\mathbf{x}, t) = \sum_k \mathbf{S}_k(\mathbf{x}) \{h_k(t - t_s)[M_{ij}(\bar{e}_{ij}^{(k)} + \Delta_p \bar{e}_{ij,p}^{(k)}) + \tilde{\Lambda}_{ijp}\bar{e}_{ij,p}^{(k)}] - h_k'(t - t_s)[M_{ij}\,\Delta t + \tilde{H}_{ij}]\bar{e}_{ij}^{(k)}\} \tag{A9}$$

where the strains $e_{ij}^{(k)}$ and strain gradient $e_{ij,p}^{(k)} = \partial_p e_{ij}^{(k)}$ are those evaluated at the fiducial point $(\mathbf{x}_s, t_s)$ and where $\Delta = \mathbf{x}_c - \mathbf{x}_s$, $\Delta t = t_c - t_s$ are the deviations of the centroid from the fiducial point.

We denote the spherical components of the moment tensors and strain tensors in geographical coordinates as follows:

$$\begin{aligned} f_1 &= M_{rr} & f_2 &= M_{\theta\theta} & f_3 &= M_{\phi\phi} \\ f_4 &= M_{r\theta} & f_5 &= M_{r\phi} & f_6 &= M_{\theta\phi} \end{aligned} \tag{A10}$$

$$\begin{array}{lll}\lambda_{11}=\bar{\Lambda}_{rrr} & \lambda_{21}=\bar{\Lambda}_{\theta\theta r} & \lambda_{31}=\bar{\Lambda}_{\phi\phi r}\\ \lambda_{41}=\bar{\Lambda}_{r\theta r} & \lambda_{51}=\bar{\Lambda}_{r\phi r} & \lambda_{61}=\bar{\Lambda}_{\theta\phi r}\\ \lambda_{12}=\bar{\Lambda}_{rr\theta} & \lambda_{22}=\bar{\Lambda}_{\theta\theta\theta} & \lambda_{32}=\bar{\Lambda}_{\phi\phi\theta}\\ \lambda_{42}=\bar{\Lambda}_{r\theta\theta} & \lambda_{52}=\bar{\Lambda}_{r\phi\theta} & \lambda_{62}=\bar{\Lambda}_{\theta\phi\theta}\\ \lambda_{13}=\bar{\Lambda}_{rr\phi} & \lambda_{23}=\bar{\Lambda}_{\theta\theta\phi} & \lambda_{33}=\bar{\Lambda}_{\phi\phi\phi}\\ \lambda_{43}=\bar{\Lambda}_{r\theta\phi} & \lambda_{53}=\bar{\Lambda}_{r\phi\phi} & \lambda_{63}=\bar{\Lambda}_{\theta\phi\phi}\end{array} \tag{A11}$$

$$\begin{array}{lll}h_1=H_{rr} & h_2=H_{\theta\theta} & h_3=H_{\phi\phi}\\ h_4=H_{r\theta} & h_5=H_{r\phi} & h_6=H_{\theta\phi}\\ \epsilon_1=e_{rr} & \epsilon_2=e_{\theta\theta} & \epsilon_3=e_{\phi\phi}\\ \epsilon_4=2e_{r\theta} & \epsilon_5=2e_{r\phi} & \epsilon_6=2e_{\theta\phi}\end{array} \tag{A12}$$

$$\begin{array}{lll}e_{11}=e_{rr;r} & e_{21}=e_{\theta\theta;r} & e_{31}=e_{\phi\phi;r}\\ e_{41}=2e_{r\theta;r} & e_{51}=2e_{r\phi;r} & e_{61}=2e_{\theta\phi;r}\\ e_{12}=e_{rr;\theta} & e_{22}=e_{\theta\theta;\theta} & e_{32}=e_{\phi\phi;\theta}\\ e_{42}=2e_{r\theta;\theta} & e_{52}=2e_{r\phi;\theta} & e_{62}=2e_{\theta\phi;\phi}\\ e_{13}=e_{rr;\phi} & e_{23}=e_{\theta\theta;\phi} & e_{33}=e_{\phi\phi;\phi}\\ e_{43}=2e_{r\theta;\phi} & e_{53}=2e_{r\phi;\phi} & e_{63}=2e_{\theta\phi;\phi}\end{array} \tag{A13}$$

where the semicolon denotes the appropriate spherical component of the Cartesian tensor $e_{ij,p}$. Equation (A9) then becomes

$$\mathbf{s}(\mathbf{x},t)=\sum_k \mathbf{S}_k\{h_k(t-t_s)[\mathbf{f}\cdot(\bar{\epsilon}+\bar{\mathbf{e}}\cdot\boldsymbol{\Delta})+\boldsymbol{\lambda}:\bar{\mathbf{e}}] - h_k'(t-t_s)(\mathbf{f}\Delta t+\mathbf{h})\cdot\bar{\epsilon}\} \tag{A14}$$

where $\boldsymbol{\Delta}$, assumed small, is given by

$$\Delta_1=\delta r_s\equiv r_c-r_s \qquad \Delta_2=r_s(\theta_c-\theta_s)\equiv r_s\delta\theta_s$$
$$\Delta_3=r_s\sin\theta_s(\phi_c-\phi_s)\equiv r_s\sin\theta_s\delta\phi_s$$

and where r_s, θ_s, ϕ_s, r_c, θ_c, ϕ_c are the geographical coordinates of $\mathbf{x}_s$, $\mathbf{x}_c$. Equation (A14) is most easily evaluated in epicentral coordinates in which θ is epicentral distance and ϕ is azimuth measured counterclockwise from south (i.e., π minus conventional azimuth of receiver from source). The appropriate expressions for $\bar{\epsilon}$ have been given by *Gilbert and Dziewonski* [1975] and are repeated in Table A1; the corresponding expressions for $\bar{\mathbf{e}}$ are also given in the table, and the notation used is defined in Table A2. Thus using the usual expressions for the eigenfunctions $\mathbf{S}_k$ in terms of scalar eigenfunctions U, V, W (see GD), (A14) leads to a straightforward evaluation of the theoretical seismograms if a catalogue of normal mode eigenfunctions is available.

It has been pointed out by *Dziewonski* [1978*b*] that the contributions to the synthetic seismograms due to a moment tensor source, for each fixed angular order l, may be expressed as linear combinations of just 10 time functions, which depend only upon the source depth, and that if these time functions are precomputed, they allow a particularly efficient evaluation of the synthetic seismograms. If it is desired to include the contributions of the second moment tensors or to calculate the kernel functions necessary in this study, the number must be extended to 25 time functions for each l, of which 10 are simply the time derivatives of the original 10. These results are obtained by performing the summation over azimuthal order m and radial order n in (A15). In this study these last 10 functions are not needed explicitly (see below).

Defining for each l the time functions $\sigma_j^{(l)}(t)$:

$$\begin{aligned}\sigma_1&=\sum_n r_s^{-1}U(r_s)U(a)h_k(t)\\ \sigma_2&=\sum_n r_s^{-1}U(r_s)V(a)h_k(t)\\ \sigma_3&=\sum_n r_s^{-1}V(r_s)U(a)h_k(t)\\ \sigma_4&=\sum_n r_s^{-1}V(r_s)V(a)h_k(t)\\ \sigma_5&=\sum_n U'(r_s)U(a)h_k(t)\\ \sigma_6&=\sum_n U'(r_s)V(a)h_k(t)\\ \sigma_7&=\sum_n V'(r_s)U(a)h_k(t)\\ \sigma_8&=\sum_n V'(r_s)V(a)h_k(t)\\ \sigma_9&=\sum_n r_sU''(r_s)U(a)h_k(t)\\ \sigma_{10}&=\sum_n r_sU''(r_s)V(a)h_k(t)\\ \sigma_{11}&=\sum_n r_sV''(r_s)U(a)h_k(t)\\ \sigma_{12}&=\sum_n r_sV''(r_s)V(a)h_k(t)\\ \sigma_{13}&=\sum_n r_s^{-1}W(r_s)W(a)h_k(t)\\ \sigma_{14}&=\sum_n W'(r_s)W(a)h_k(t)\\ \sigma_{15}&=\sum_n r_sW''(r_s)W(a)h_k(t)\end{aligned} \tag{A15}$$

(A14) can be written

$$s_k(\mathbf{x},t)=\sum_l\sum_j\left(\sigma_j^{(l)}\sum_i\left[c_j^{kl}f_i+\sum_p(f_i\Delta_p+\lambda_{ip})d_j^{klp}\right]+\dot{\sigma}_j^{(l)}\sum_i(f_i\Delta t+h_i)c_j^{ki}\right) \tag{A16}$$

where $k=1, 2, 3$ refers to radial, longitudinal, and transverse components. The coefficients c_j^{ki}, d_j^{klp} depend upon the epicentral distance and azimuth and also upon l; for the sake of brevity we do not list them explicitly here.

It is clearly feasible and desirable to use (A16) to attempt to place constraints upon the second moment tensors $\bar{\Lambda}$, $\bar{H}$, which are subject to the constraints [*Backus*, 1977]

$$M_{ij}\bar{\Lambda}_{ijp}=0 \qquad M_{ij}\bar{H}_{ij}=0$$

In the present study, however, it has been assumed that their contributions are small, and (A16) has been used to solve the

TABLE A1. Expressions for $\bar{\mathbf{e}}$ [*Gilbert and Dziewonski, 1975*] and Corresponding Expressions for $\bar{\mathbf{e}}$

	Spheroidal Modes				Toroidal Modes			
	$m=0$	$m=\pm1$	$m=\pm2$	$m=\pm3$	$m=0$	$m=\pm1$	$m=\pm2$	$m=\pm3$
$\bar{e}_1$	$k_0\dot{U}$							
$\bar{e}_2$	$\frac{1}{2}k_0F$		$k_2r^{-1}V$				$\mp ik_2r^{-1}W$	
$\bar{e}_3$	$\frac{1}{2}k_0F$		$-k_2r^{-1}V$				$\pm ik_2r^{-1}W$	
$\bar{e}_4$		$-k_1E_S$				$\pm ik_1E_T$		
$\bar{e}_5$		$\pm ik_1E_S$				E_Tk_1		
$\bar{e}_6$			$\mp2ik_2r^{-1}V$				$-2k_2r^{-1}W$	
$\bar{e}_{11}$	$k_0\dot{U}$							
$\bar{e}_{21}$	$-k_0p_5$		k_2p_4				$\pm ik_2q_1$	
$\bar{e}_{31}$	$-k_0p_5$		$-k_2p_4$				$\mp ik_2q_1$	
$\bar{e}_{41}$		$-k_1(\dot{V}+p_1)$				$\pm ik_1(\dot{W}+q_1)$		
$\bar{e}_{51}$		$\pm ik_1(\dot{V}+p_1)$				$k_1(\dot{W}+q_1)$		
$\bar{e}_{61}$			$\mp2ik_2p_4$				$2k_2q_1$	
$\bar{e}_{12}$		$-k_1p_1$				$\pm ik_1q_1$		
$\bar{e}_{22}$		$k_1(p_6+p_7)$		$-k_3r^{-2}V$		$\mp ik_1(q_6+q_7)$		$\pm ik_3r^{-2}W$
$\bar{e}_{32}$		k_1p_7		$k_3r^{-2}V$		$\mp ik_1q_7$		$\mp ik_3r^{-2}W$
$\bar{e}_{42}$	$k_0(p_3-p_5)$		$k_2(p_2+p_4)$				$\mp ik_2(q_2-q_1)$	
$\bar{e}_{52}$			$\mp ik_2(p_2+p_4)$		k_0q_5		$-k_2(q_2-q_1)$	
$\bar{e}_{62}$		$\mp ik_1p_6$		$\pm2ik_3r^{-2}V$		$-k_1q_6$		$2k_3r^{-2}W$
$\bar{e}_{13}$		$\pm ik_1p_1$				k_1q_1		
$\bar{e}_{23}$		$\mp ik_1p_7$		$\pm ik_3r^{-2}V$		$-k_1q_7$		$k_3r^{-2}W$
$\bar{e}_{33}$		$\mp ik_1(p_6+p_7)$		$\mp ik_3r^{-2}V$		$-k_1(q_6+q_7)$		$-k_3r^{-2}W$
$\bar{e}_{43}$			$\mp ik_2(p_2+p_4)$		$-k_0q_5$		$-k_2(q_2-q_1)$	
$\bar{e}_{53}$	$k_0(p_3-p_5)$		$-k_2(p_2+p_4)$				$\pm ik_2(q_2-q_1)$	
$\bar{e}_{63}$		k_1p_6		$2k_3r^{-2}V$		$\mp ik_1q_6$		$\mp2ik_3r^{-2}W$

simpler inverse problem for Δ, Δt. Neglecting the contributions from λ, $\mathbf{h}$, we have

$$s_k(\mathbf{x},t)=\sum_i(\psi_{ki}f_i)+b_k\delta r_s+c_k\delta\theta_s+d_k\delta\phi_s+e_k\delta t_s \qquad \text{(A17)}$$

where

$$\psi_{ki}=\psi_k(t)=\sum_l\sum_j\sigma_j^{(l)}c_j^{kl}$$

$$b_k=\sum_l\sum_j\sigma_j^{(l)}\sum_i f_id_j^{kl1}$$

$$c_k=r_s\sum_l\sum_j\sigma_j^{(l)}\sum_i f_id_j^{kl2}$$

$$d_k=r_s\sin\theta_s\sum_l\sum_j\sigma_j^{(l)}\sum_i f_id_j^{kl3}$$

$$e_k=-\sum_l\sum_j\dot{\sigma}_j^{(l)}\sum_i f_ic_j^{kl}$$

TABLE A2. Notation Used in Table A1

Spheroidal Modes	Toroidal Modes
$F=r^{-1}[2U-l(l+1)V]$	
$E_S=\dot{V}-r^{-1}(V-U)$	$E_T=\dot{W}-r^{-1}W$
$p_1=r^{-1}(\dot{U}-\dot{V}-r^{-1}U+r^{-1}V)$	$q_1=-r^{-1}(\dot{W}-r^{-1}W)$
$p_2=r^{-2}(U-2V)$	$q_2=-2r^{-2}W$
$p_3=r^{-1}[\dot{U}-r^{-1}U+\frac{1}{2}r^{-1}l(l+1)(2V-U)]$	
$p_4=r^{-1}(\dot{V}-r^{-1}V)$	
$p_5=r^{-1}[\frac{1}{2}l(l+1)(\dot{V}-r^{-1}V)-\dot{U}+r^{-1}U]$	$q_5=\frac{1}{2}r^{-1}l(l+1)(\dot{W}-r^{-1}W)$
$p_6=r^{-1}[\frac{1}{2}r^{-1}l(l+1)V-\dot{V}-r^{-1}U]$	$q_6=r^{-1}[\frac{1}{2}r^{-1}l(l+1)W-\dot{W}]$
$p_7=-r^{-2}\{\frac{1}{2}[l(l+1)-2]V+\frac{1}{2}rF\}$	$q_7=-\frac{1}{2}r^{-2}[l(l+1)-2]W$

U, V, W to be evaluated at radius $r=|\mathbf{x}_0|$. Parameter $k_n=(1/2^n)\{[(2l+1)/4\pi][((l+n)!)/((l-n)!)]\}^{1/2}$, i.e., $k_0=[(2l+1)/4\pi]^{1/2}$; $k_n=\frac{1}{2}[(l+n)(l-n+1)]^{1/2}k_{n-1}$.

When a starting solution for the moment tensor $f^{(0)}$ has been found, (A17) may be used iteratively to simultaneously improve the location and moment tensor solutions as described in section 2*c*. It will be noticed that $-e_k(t)$ is simply the time derivative of the first term in (A17). In the iterative procedure of section 2*c* the spectrum of this term is available from the previous iteration, and since differentiation is readily performed in the frequency domain, explicit calculation of e_k is not necessary.

Acknowledgments. We would like to thank T. J. Fitch and R. G. North of the Applied Seismology Group, Lincoln Laboratory, MIT, for discussions and help in accessing the data from the SRO/ASRO network. In particular, Tom Fitch drew our attention to the delayed aftershock series of the Sumba earthquake. We have profited greatly from numerous discussions with H. Kanamori of Caltech; in this paper we have followed several of his suggestions. F. Gilbert and G. Masters of the University of California, San Diego, shared with us their experience in retrieving the source mechanism from a network of stations with digital recordings. R. P. Buland of the USGS made available to us his catalog of normal modes which we have used throughout this study. Diane DeAngelis contributed greatly to the final form of this report. This research was supported by a grant EAR76-14839 from the National Science Foundation.

REFERENCES

Agnew, D., J. Berger, R. Buland, W. Farrell, and F. Gilbert, International deployment of accelerometers: A network of very long period seismology, *Eos Trans. AGU, 57*, 180–188, 1976.

Aki, K., Generation and propagation of *G* waves from the Niigata earthquake of June 16, 1964, *Bull. Earthquake Res. Inst. Tokyo Univ., 44*, 23–88, 1966.

Aki, K., Scaling law of seismic spectrum, *J. Geophys. Res., 72*, 1217–1231, 1967.

Aki. K., and H. Patton, Determination of seismic moment tensor using surface waves, *Tectonophysics, 49*, 213–222, 1978.

Backus, G. E., Interpreting the seismic glut moments of total degree two or less, *Geophys. J. R. Astron. Soc., 51*, 1–25, 1977.

Backus, G. E., and M. Mulcahy, Moment tensors and other phenome-

nological descriptions of seismic sources, I, Continuous displacements, *Geophys. J. R. Astron. Soc., 46,* 341–361, 1976.
Ben-Menahem, A., Radiation of seismic surface waves from finite moving sources, *Bull. Seismol. Soc. Am., 51,* 401–435, 1961.
Buland, R. P., Retrieving the seismic moment tensor, Ph.D. thesis, Univ. of Calif., San Diego, 1976.
Buland, R., and F. Gilbert, Matched filtering for seismic moment tensor, *Geophys. Res. Lett., 3,* 205–206, 1976.
Buland, R., J. Berger, and F. Gilbert, Observations of attenuation and splitting from the IDA network, *Nature, 277,* 358–362, 1979.
Chen, T., and D. W. Forsyth, A detailed study of two earthquakes seaward of the Tonga trench: Implications for mechanical behavior of the oceanic lithosphere, *J. Geophys. Res., 83,* 4995–5003, 1978.
Denham, D., Summary of earthquake focal mechanisms for the western Pacific-Indonesian region, 1929–1973, *Rep. SE-3,* World Data Cent. A, Boulder, Colo., 1977.
Dziewonski, A. M., Finite strain Earth model with consideration of velocity dispersion due to anelasticity, in Seismic Discrimination, Semiannual Technical Summary, pp. 94–98, Lincoln Lab., Mass. Inst. of Technol., Cambridge, 1977.
Dziewonski, A. M., Rapid computation of synthetic seismograms by superposition of normal modes (abstract), *Eos Trans. AGU, 59,* 325, 1978*a*.
Dziewonski, A. M., Synthetic seismograms by superposition of normal modes: Application to the inverse problem for source mechanism, in Semiannual Technical Summary, Applied Seismology Group, pp. 23–27, 40–42, Lincoln Lab., Mass. Inst. of Technol., Cambridge, 1978*b*.
Dziewonski, A. M., and F. Gilbert, Temporal variation of the seismic moment and the evidence of precursive compression for two deep earthquakes, *Nature, 247,* 185–188, 1974.
Engdahl, E. R., *Global Earthquake Monitoring: Its Uses, Potentials and Support Requirements,* report of the Panel on Seismograph Networks, Committee on Seismology, National Academy of Sciences, Washington, D. C., 1977.
Engdahl, E. R., and H. Kanamori, Determination of earthquake parameters, *Eos Trans. AGU, 61,* 62–64, 1980.
Fitch, T. J., D. W. McCowan, and M. W. Shields, Estimation of the seismic moment tensor from teleseismic body wave data with applications to intraplate and mantle earthquakes, *J. Geophys. Res., 85,* 3817–3828, 1980.
Fitch, T. J., R. G. North, and M. W. Shields, Focal depths and moment tensor representations of shallow earthquakes associated with the great Sumba earthquake, submitted to *J. Geophys. Res.,* 1981.
Gilbert, F., Excitation of the normal modes of the Earth by earthquake sources, *Geophys J. R. Astron. Soc., 22,* 223–226, 1971.
Gilbert, F., Derivation of source parameters from low-frequency spectra, *Philos. Trans. R. Soc. London, 274,* 369–371, 1973.
Gilbert, F., and R. Buland, An enhanced deconvolution procedure for retrieving the seismic moment tensor from a sparse network, *Geophys. J. R. Astron. Soc., 50,* 251–255, 1976.
Gilbert, F., and A. M. Dziewonski, An application of normal mode theory to the retrieval of structural parameters and source mechanisms from seismic spectra, *Philos. Trans. R. Soc. London, Ser. A, 278,* 187–269, 1975.
Hales, A. L., and H. A. Doyle, *P* and *S* travel time anomalies and their interpretation, *Geophys. J. R. Astron. Soc., 13,* 403–415, 1967.
Isacks, B., and P. Molnar, Distribution of stresses in the descending lithosphere from a global survey of focal mechanism solution of mantle earthquakes, *Rev. Geophys. Space Phys., 9,* 103–174, 1971.
Isacks, B., J. Oliver, and L. R. Sykes, Seismology and the new global tectonics, *J. Geophys. Res., 73,* 5855–5899, 1968.
Kanamori, H., Synthesis of long-period surface waves and its applications to earthquake source studies—Kurile Islands earthquake of October 13, 1963, *J. Geophys. Res., 75,* 5011–5028, 1970*a*.
Kanamori, H., The Alaska earthquake of 1964: Radiation of long-period surface waves and source mechanism, *J. Geophys. Res., 75,* 5029–5040, 1970*b*.
Kanamori, H., Quantification of earthquakes, *Nature, 271,* 411–414, 1978.
Kanamori, H., Use of IDA network for fast determination of earthquake source parameters (abstract), *Eos Trans. AGU, 61,* 296, 1980.
Kanamori, H., and D. L. Anderson, Theoretical basis of some empirical relations in seismology, *Bull. Seismol. Soc. Am., 65,* 1073–1095, 1975.
Kanamori, H., and G. S. Stewart, Mode of the strain release along the Gibbs fracture zone, Mid-Atlantic Ridge, *Phys. Earth Planet. Inter., 11,* 312–332, 1976.
Knopoff, L., and M. J. Randall, The compensated linear-vector dipole: A possible mechanism for deep earthquakes, *J. Geophys. Res., 75,* 4957–4963, 1970.
Langston, C. A., and D. W. Helmberger, A procedure for modelling shallow dislocation sources, *Geophys. J. R. Astron. Soc., 42,* 117–130, 1975.
Liu, H.-P., D. L. Anderson, and H. Kanamori, Velocity dispersion due to anelasticity: Implications for seismology and mantle composition, *Geophys. J. R. Astron. Soc., 47,* 41–58, 1976.
Masters, G., and F. Gilbert, Source retrieval from a sparse long period network (abstract), *Eos Trans. AGU, 60,* 879, 1979.
Melosh, H. J., Nonlinear stress propagation in the earth's upper mantle, *J. Geophys. Res., 81,* 5621–5632, 1976.
Okal, E. A., and D. L. Anderson, A study of lateral heterogeneities in the upper mantle by multiple *ScS* travel time residuals, *Geophys. Res. Lett., 2,* 313–316, 1975.
Patton, H. J., Source and propagation effects of Rayleigh waves from central Asian earthquakes, Ph.D. thesis, Mass. Inst. of Technol., Cambridge, 1978.
Patton, H. J., Reference point equalization method for determining the source and path effects of surface waves, *J. Geophys. Res., 85,* 821–848, 1980.
Peterson, J., H. M. Butler, L. G. Holcomb, and C. R. Hutt, The seismic research observatory, *Bull. Seismol. Soc. Am., 66,* 2049–2068, 1976.
Randall, M. J., and L. Knopoff, The mechanism at the focus of deep earthquakes, *J. Geophys. Res., 75,* 4965–4976, 1970.
Saito, M., Excitation of free oscillations and surface waves by a point source in a vertically heterogeneous earth, *J. Geophys. Res., 72,* 3689–3699, 1967.
Sipkin, S. A., and T. H. Jordan, Lateral heterogeneity of the upper mantle determined from the travel times of *ScS, J. Geophys. Res., 80,* 1474–1484, 1975.
Sipkin, S. A., and T. H. Jordan, Lateral heterogeneity of the upper mantle determined from the travel times of multiple *ScS, J. Geophys. Res., 81,* 6307–6320, 1976.
Sipkin, S. A., and T. H. Jordan, Multiple *ScS* travel times in the western Pacific: Implications for mantle heterogeneity, *J. Geophys. Res., 85,* 853–861, 1980.
Stewart, G. S., Implications for plate-tectonics of the Aug. 19, 1977 Indonesian decoupling normal-fault earthquakes (abstract), *Eos Trans. AGU, 59,* 326, 1978.
Stump, B. W., and L. R. Johnson, The determination of source properties by the linear inversion of seismograms, *Bull. Seismol. Soc. Am., 67,* 1489–1502, 1977.
Sykes, L. R., Mechanism of earthquakes and nature of faulting on the mid-oceanic ridge, *J. Geophys. Res., 72,* 2131–2153, 1967.
Ward, S., A technique for the recovery of the seismic moment tensor applied to the Oaxaca, Mexico earthquake of November 1978, *Bull. Seismol. Soc. Am., 70,* 717–734, 1980.

(Received August 11, 1980;
revised October 17, 1980;
accepted November 7, 1980.)